CONTRIBUTIONS TO AN IMPROVED OXYGEN AND THERMAL TRANSPORT MODEL AND DEVELOPMENT OF FATIGUE ANALYSIS SOFTWARE FOR ASPHALT PAVEMENTS

A Thesis

by

XIN JIN

Submitted to the Office of Graduate Studies of
Texas A&M University
in partial fulfillment of the requirements for the degree of

MASTER OF SCIENCE

August 2009

Major Subject: Chemical Engineering

CONTRIBUTIONS TO AN IMPROVED OXYGEN AND THERMAL TRANSPORT MODEL AND DEVELOPMENT OF FATIGUE ANALYSIS SOFTWARE FOR ASPHALT PAVEMENTS

A Thesis

by

XIN JIN

Submitted to the Office of Graduate Studies of
Texas A&M University
in partial fulfillment of the requirements for the degree of

MASTER OF SCIENCE

Approved by:

Chair of Committee,	Charles J. Glover
Committee Members,	Victor M. Ugaz
	Amy Epps Martin
Head of Department,	Michael Pishko

August 2009

Major Subject: Chemical Engineering

ABSTRACT

Contributions to an Improved Oxygen and Thermal Transport Model and Development of Fatigue Analysis Software for Asphalt Pavements.

(August 2009)

Xin Jin, B. E., Zhejiang University

Chair of Advisory Committee: Dr. Charles J. Glover

Fatigue cracking is one primary distress in asphalt pavements, dominant especially in later years of service. Prediction of mixture fatigue resistance is critical for various applications, e.g., pavement design and preventative maintenance. The goal of this work was to develop a tool for prediction of binder aging level and mixture fatigue life in pavement from unaged binder/mixture properties. To fulfill this goal, binder oxidation during the early fast-rate period must be understood. In addition, a better hourly air temperature model is required to provide accurate input for the pavement temperature prediction model. Furthermore, a user-friendly software needs to be developed to incorporate these findings.

Experiments were conducted to study the carbonyl group formation in one unmodified binder (SEM 64-22) and one polymer-modified binder (SEM 70-22), aged at five elevated temperatures. Data of SEM 64-22, especially at low temperatures, showed support for a parallel-reaction model, one first order reaction and one zero order reaction. The model did not fit data of SEM 70-22. The polymer modification of SEM

70-22 might be responsible for this discrepancy. Nonetheless, more data are required to draw a conclusion.

Binder oxidation rate is highly temperature dependent. Hourly air temperature data are required as input for the pavement temperature prediction model. Herein a new pattern-based air temperature model was developed to estimate hourly data from daily data. The pattern is obtained from time series analysis of measured data. The new model yields consistently better results than the conventional sinusoidal model.

The pavement aging and fatigue analysis (PAFA) software developed herein synthesizes new findings from this work and constant-rate binder oxidation and hardening kinetics and calibrated mechanistic approach with surface energy (CMSE) fatigue analysis algorithm from literature. Input data include reaction kinetics parameters, mixture test results, and pavement temperature. Carbonyl area growth, dynamic shear rheometer (DSR) function hardening, and mixture fatigue life decline are predicted as function of time. Results are plotted and saved in spreadsheets.

ACKNOWLEDGEMENTS

I would like to thank my committee chair, Dr. Glover, and my committee members, Dr. Ugaz and Dr. Epps Martin, for their guidance and support throughout the course of this research.

This work would not be possible without the extensive help from my co-workers, Nikornpon Prapaitrakul, Rongbin Han, and Yuanchen Cui, who assisted in data collection and analysis.

Thanks also go to my friends and colleagues and the department faculty and staff for making my time at Texas A&M University a great experience.

Finally, thanks to my mother and father for their encouragement and to my wife for her patience and love.

TABLE OF CONTENTS

CHAPTER Page

LIST OF FIGURES

FIGURE Page

FIGURE Page

LIST OF TABLES

TABLE Page

CHAPTER I

INTRODUCTION

Background

According to Federal Highway Administration's publication *Highway Statistics 2007* (*1*), in the United States about 2.5 million miles road are surfaced with asphalt concrete at of a total of approximately 4 million miles. Due to repeated traffic loading and cyclic pavement temperature change, asphalt pavements will suffer from three primary stresses, namely permanent deformation or rutting, thermal cracking, and fatigue cracking. Rutting usually occurs during the early years of pavement life, while fatigue cracking manifests itself in later years. To ensure satisfactory pavement performance and to reduce the overall maintenance cost, it is imperative that pavement maintenance agencies know the status of the pavement and find the optimal time for maintenance application.

One way to establish good pavement performance is to select a qualified binder and design a good mixture. After five years of research, the Strategic Highway Research Program (SHRP) developed the Superpave (Superior Performing Asphalt Pavement) protocol system, which consists of a binder performance grading (PG) specification and a mixture design. The PG grading of binder is based on binder tests at critical temperatures related to rutting, thermal cracking, and fatigue cracking. The high and low

_____

This thesis follows the style of *Transportation Research Record*.

PG grades of binder are determined from high-temperature complex elasticity measurement and low-temperature stiffness and failure measurements. Therefore, PG grade is designed to ensure binder performance against rutting and thermal cracking. Although PG grading does include a test of fatigue resistance, that test does not control PG grade because it runs at intermediate temperature. Hence, it is impossible to tell binder fatigue performance from PG grades. In addition, Superpave mixture design does not have a mixture test on fatigue performance. In summary, fatigue characterization and analysis of binder and mixture are needed to address fatigue cracking in pavement. Such a need is partially satisfied by the Mechanistic-Empirical Pavement Design Guide (MEPDG).

MEPDG is a software program based on mechanistic empirical design procedure. It provides an interface to input design variables and to predict pavement performance. The design procedure incorporates the effect of pavement temperature, moisture, and binder aging on material properties, in addition to variations of traffic loadings. Models for the three primary stresses (rutting, thermal cracking and fatigue cracking) are all formulated in design procedure. Although such a tool is in great need, its application is quite challenging because its empirical basis asks for extensive field calibration. Moreover, its reliability is blighted by some fundamental problems associated with the models.

The global aging model (GAM) developed by Mirza and Witczak (*2*) is adopted by MEPDG to model asphalt aging in pavements. The aging process is modeled into two parts, short-term aging and long-term aging. Accordingly, asphalt properties are

classified into three stages: original properties from refinery, mix/laydown (short-term) properties after plant mixing and laydown operation, and field aged (long-term) properties in the long run. Three models are developed to 1) predict mix/laydown viscosity from the original viscosity; 2) predict field aged viscosity from short-term viscosity; and 3) predict long-term properties as a function of depth. While the scheme of the models is appropriate, several underlying assumptions are quite problematic.

First, the GAM is a statistical model based on measurements of physical properties (viscosity and penetration). Data used for regression are from various binder types and different test systems. The result is a generic model that is taken as valid for all unmodified binders, specifically, Shell Oil category straight run binders. However, an extensive laboratory study of binder aging (*3*) shows that each type of binder has unique binder aging kinetics, leading to different aging rates and different physical properties. Thus a big disadvantage of GAM is the lack of support from fundamental chemical analysis. Second, environmental temperature is considered, but in a superficial way. GAM used mean annual air temperature to reflect the significant effect of environmental conditions. However, solar radiation, the most important factor that affects pavement temperature and binder aging rate, is not mentioned. In addition, the mean annual temperature is not representative of temperature effect. The fluctuation of pavement temperature, yearly and daily, does not cancel out its effect on binder aging because the aging rate is not a linear function of pavement temperature. Last but not least, although GAM realized the relationship of viscosity and depth, the conclusion that aging can be ignored below the top one inch of asphalt layer is contradictory to experimental data

from Al-Azri et al. (*4*).

Beside GAM, the fatigue cracking model in MEPDG is also questionable. The mathematical form of the model is shown in Equation 1-1.

$$N_f = N_i + N_p = N_i + (C-1)\cdot N_i = C \cdot N_i \quad (1\text{-}1)$$

where N_f is number of loading cycles to fatigue failure, N_i is number of loading cycles for crack initiation, N_p is number of loading cycles for crack propagation and C is a shift factor.

Note fatigue cracking is a two-stage process, which consists of crack initiation and crack propagation. Equation 1-1 assumes crack propagation can be linearly related to crack initiation by a factor of (C−1). However, fracture mechanics based on the Paris Law (*5*) shows that they should be characterized individually. Moreover, the effect of binder aging has not been incorporated into the model.

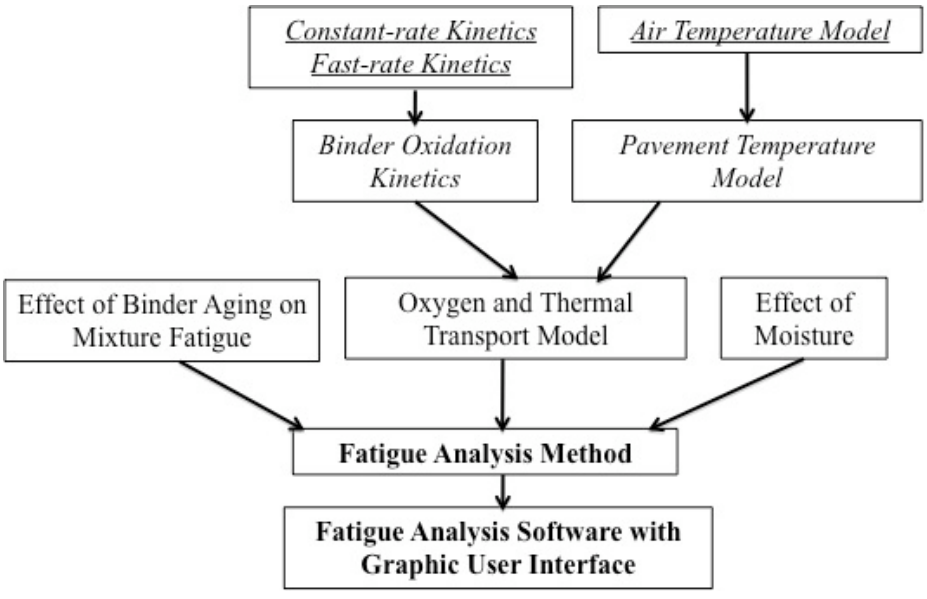

FIGURE 1-1 Overview of a better fatigue analysis system.

Overview of Fatigue Analysis System

To address the limitations of MEPDG models, a better fatigue analysis system is designed, as shown in Figure 1-1. The heart of the fatigue analysis system is the fatigue analysis method based on mechanistic theory. The system should include an oxygen and thermal transport model that describes how binder ages in pavement depending on pavement temperature and oxygen accessibility. It should also incorporate the effect of binder aging on mixture fatigue performance and the effect of moisture. Finally, it should provide a user-friendly software interface for easy application.

Objectives

The ultimate objective of this work is to improve the fatigue analysis system for prediction of binder oxidation in pavement and mixture fatigue life. The limitations of GAM and fatigue cracking model adopted in MEPDG will be addressed. These include better characterization of binder oxidation from production throughout pavement service, accurate prediction of pavement temperature, and application of a recently developed fatigue analysis method.

Specifically, the objectives of this research include:

1. To develop binder oxidation kinetics model in terms of carbonyl formation during the early period of binder aging that includes the effect of aging temperature.
2. To model hourly air temperature for the purposes of hourly pavement temperature calculation.
3. To develop pavement aging and fatigue analysis software with a graphic user

interface that incorporates more fundamental understanding of binder aging and mixture fatigue characterization.

Literature Review

The literature review on asphalt aging and mixture fatigue performance are presented in three major parts: binder oxidation kinetics, oxygen and thermal transport model, and calibrated mechanistic surface energy (CMSE) approach for mixture fatigue analysis.

Binder Oxidation Kinetics

To understand how binder ages, it is important to know its composition. Modern asphalt binder is a bottom product from the petroleum crude oil refinery industry. Some (*6*) estimated that it is composed by millions of chemical species. In general, asphalt can be categorized into three major components: asphaltene, resin, and maltene. Some components react with oxygen and form products that make the binder stiffer. The most important products are carbonyl functional group (or ketones) and sulfoxides (*3, 7*). These two products, especially carbonyl group, are major contributors to binder hardening.

The formation of carbonyl functional group (C=O) is measured using Fourier transform infrared spectroscopy (FT-IR), and defined quantitatively as the integral area of carbonyl region from 1,650 to 1,820 cm^{-1} of FTIR spectrum. This area is named carbonyl area (CA). Figure 1-2 shows the growth of carbonyl area. The separation of spectroscopy of neat asphalt (bottom line) and aged asphalts (top line) clearly shows the increase of carbonyl area.

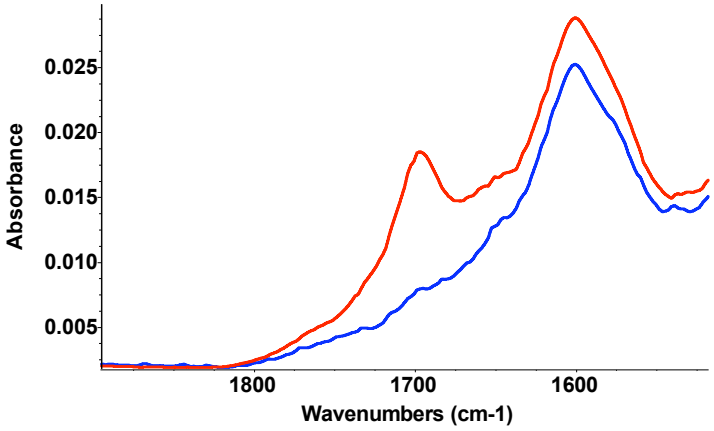

FIGURE 1-2 FTIR spectroscopy for neat and aged asphalts.

Domke et al. (*8*) studied the chemical-physical relationship of binder. They aged several types of binder under different aging conditions and found that low shear rate limiting viscosity increases linearly with carbonyl area. They termed the slope as viscosity hardening susceptibility (HS). Experimental data show that viscosity HS is binder source dependent, oxygen pressure dependent, but not temperature dependent.

In addition to carbonyl area and viscosity, the logarithm of dynamic shear rheometer (DSR) function G'/(η'/G'), which relates well to binder ductility under 10 cm, also increases linearly with carbonyl formation (*9*). Note that DSR function includes both the dynamic elastic modulus (G') and viscosity (η') of the binder and correlates to binder durability.

Binder usually oxidizes in two stages, a fast-rate period and a constant-rate period. Most previous work (*3, 8, 9*) focus on constant-rate kinetics of binder oxidation, because the duration of the fast-rate period is assumed to be short and will not affect

long-term performance, especially in the laboratory under elevated temperature and oxygen pressure. The carbonyl formation rate during the constant-rate period is:

$$r = A \cdot P^{\alpha} \cdot e^{(-E_a / RT)} \tag{1-2}$$

where A is the frequency factor, P is oxygen pressure, α is the reaction order with respect to oxygen pressure, E_a is the activation energy, R is the gas constant, and T is the absolute temperature (K). Apparently, the rate of carbonyl formation, or equivalently, the rate of oxidation, is dependent on oxygen pressure, temperature, and activation energy. Binders from different sources have different activation energies and reaction order, and thus different aging rates.

While the constant-rate kinetics have been studied extensively, the early-time, fast-rate period reaction kinetics have been studied much less. Although the termination of fast-rate period of oxidation in the laboratory can be assured, it is more difficult to tell when it ends in the field due to the lower and cyclical field temperatures in pavements, especially those in cold climate region. Using constant-rate period kinetics to assess field aging without knowing if the fast-rate period has been passed may contribute considerable error and uncertainty to the results and conclusions. Thus, in Chapter II of this work, the experiment is designed to understand fast-rate aging kinetics of asphalt binder and the effect of temperature.

Thermal and Oxygen Transport Model in Pavement

As expressed in Equation 1-2 of constant-rate kinetics, the rate of binder oxidation is temperature and oxygen partial pressure dependent, and it increases with

temperature exponentially. In order to model binder oxidation in pavement, it is important to know pavement temperature as a function of time and depth.

Measured hourly pavement temperature data varying with time and depth are available through the Long Term Performance Program (LTPP) database. The data are limited in terms of pavement location and time range. Most states have data available for only one or two sites, and missing data are common over an entire year. Nonetheless, they are invaluable for the study and modeling of pavement temperature.

For pavement sites for which measured data are unavailable, data can be predicted using models. Several models for this purpose had been presented in literature (*10~13*). One method (*10*) uses a heat transfer model with a surface periodic temperature boundary condition assuming that daily and annual pavement temperatures are sinusoidal functions of time. The resulting model yields an analytical solution of pavement temperature versus depth over time. However, this model requires pavement surface temperature data as an input, which is usually not available. In addition, due to over-simplification, the results are not accurate. Diefenderfer et al. (*11*) use a statistical regression model to establish pavement maximum and minimum temperatures as a function of depth. This model takes into account solar radiation and ambient air temperature. Complete hourly temperature profiles, however, are not obtained. In addition, this model assumes a linear dependence of pavement temperature on depth, which is fundamentally wrong and experimentally inconsistent with measured data.

A more sophisticated model also uses a heat transfer model, but assumes a surface heat flux boundary condition and employs a finite different approximation to

obtain a numerical solution; hourly temperature data are obtained (*12, 13*). The prediction results show good agreement with measured data from the LTPP database. The maximum of monthly average absolute error is 2.0 °C (*13*).

The disadvantage of model prediction is the cost of computation time and the acquisition of various input data. These inputs include hourly solar radiation, hourly air temperature, and wind speed data. In Chapter III of this thesis, a new pattern-based air temperature model is developed. This model is compared with conventional sinusoidal model.

The pavement temperature model is not integrated into the software developed in Chapter IV, because that is not the objective of the software. But pavement temperature data are required as input for the software. Thus, it is assumed that user has pavement temperature available, measured or calculated, before using the software.

Oxygen pressure data, compared to temperature data, are more difficult to obtain. It is almost impractical to measure oxygen pressure directly in a pavement. It is also challenging to build a model that can take into account the heterogeneity of asphalt-aggregate mixture and the complex distribution of air voids. Despite these difficulties, work (*14, 15, 16*) is being done to fulfill the modeling of oxygen transport and reaction in pavement.

Lunsford (*14*) built a model for oxygen transport and reaction in flat, one-dimensional asphalt film. The model is described by Equation 1-3.

$$(\frac{\partial P}{\partial t}) = (\frac{\partial D_{O_2}}{\partial x})(\frac{\partial P}{\partial x}) + D_{O_2}(\frac{\partial^2 P}{\partial x^2}) - (\frac{cRT}{h})r_{CA} \quad (1\text{-}3)$$

In this equation, P is oxygen partial pressure; D_{O_2} is oxygen diffusivity in pure binder; h is Henry's law constant, relating oxygen partial pressure at binder film surface to oxygen concentration in binder film surface; r_{CA} is the rate of carbonyl formation; and c is a constant that relates r_{CA} to the rate of oxygen consumption.

The most important parameter that needs to be measured is oxygen diffusivity. Equation 1-3 is simplified to facilitate the measurement, by assuming steady state in oxygen pressure and a constant oxygen diffusivity. This leads to a simplified equation.

$$0 = D_{O_2}(\frac{\partial^2 P}{\partial x^2}) - (\frac{cRT}{h})r_{CA} \quad (1\text{-}4)$$

This equation provides a theoretical basis for oxygen diffusivity measurement. Lunsford aged 1 mm films at constant pressure and measured the carbonyl area growth rate at the bottom layer of the film. Using these data, oxygen pressure at the bottom layer can be calculated from binder aging kinetics, assuming reaction order with respect to pressure as 0.27. This provides an additional boundary condition from which oxygen diffusivity can be estimated.

One thing that complicates the oxygen diffusivity measurement is the effect of binder aging. Generally, as binder ages, it becomes stiffer and thus more difficult for the oxygen to diffuse in the binder. Lunsford related D_{O_2} to zero shear rate viscosity η_0^* (poise) by

$$D_{O_2} = D_0(\eta_0^*)^B \quad (1\text{-}5)$$

where D_0 (m^2/s) is diffusivity of neat binder, and B is -0.84 for asphalt, as estimated by Lunsford.

While Lunsford's model is indispensable for study of binder aging in thin film and for estimation of oxygen diffusivity, it cannot be applied directly to oxygen diffusion in asphalt concrete in field study. First, in mixture, oxygen is actually diffusing in binder-filler mastics; thus the diffusivity value measured in pure binder requires calibration. Second, X-ray computed tomography (CT) of mixtures by Al-Omari et al. (*15*) suggests a cylindrical air void channel instead of flat asphalt-air surface. Finally, the aggregates in mixture serve as obstacles to oxygen, preventing oxygen diffusion freely through the mixture.

Recently, Prapaitrakul et al. (*16*) developed a model that addresses the last two complications. A more realistic, cylindrical geometry for air voids is used based on extensive X-ray CT images, which leads to a partial differential equation in a cylindrical system.

$$(\frac{\partial P}{\partial t}) = \frac{1}{r}\frac{\partial}{\partial r}\left(rD_{O_2}\frac{\partial P}{\partial r}\right) - (\frac{cRT}{h})r_{CA} \tag{1-6}$$

Furthermore, the effect of aggregates is considered via the concept of effective diffusivity.

$$D_e = D_{O_2} \cdot \frac{\varepsilon}{\tau} \tag{1-7}$$

where ε is porosity and τ is tortuosity.

In this thesis, Prapaitrakul's model will be incorporated into the software developed in Chapter IV, although the model is based on preliminary experimental data and needs further validation. In addition, oxygen diffusivity for pure binder will be used, because data for mastic are not available.

CMSE Fatigue Analysis System

Fatigue resistance of pavement, as an important pavement performance property, is of great interest to mixture designers. Several mixture fatigue analysis systems have been developed to evaluate mixture fatigue life. Most of them are mechanistic-empirical based. They assume an empirical relationship between fatigue life and applied tensile strain, while the critical design stress or strain within the pavement structure is often determined from multi-layer elasticity theory. The MEPDG also adopts a semi-empirical approach for structural design of flexible pavement.

Over the past decade, the shift from empirical fatigue analysis approaches to a more mechanistic one has been emphasized. A mechanistic based approach requires only fundamental material properties determined from laboratory tests. Researchers (*17*) recommended the use of dissipated energy and fracture mechanics instead of an empirical fatigue relationship. The CMSE method summarized in TxDOT project 0-4468 (*17*) is the first fatigue analysis method based on fundamental continuum micromechanics. It is proved to be able to produce comparable results as MEPDG. The following sections provide a brief review on CMSE method.

Hot mix asphalt concrete (HMAC) is a complex heterogeneous material, consisting of solid aggregate, visco-elastic asphalt binder, and air voids. It behaves as a non-linear visco-elastic composite material. Repeated traffic loading induces fatigue cracking in HMAC. Under each loading cycle, energy is stored on crack faces due to viscous lag in material response, driving the fracture process. This energy is called dissipated pseudo strain energy (DPSE). Under repeated loading, DPSE will increase,

which means more and more damage is accumulated on crack faces. At the meantime, HMAC undergoes a healing process during rest period between loading cycles. At the absence of traffic loading, fracture surface tends to close and a certain amount of energy is released.

The CMSE approach treats individually the two stages of the fracture process, crack initiation and crack propagation. The number of loading cycles for crack initiation, N_i, and number of loading cycles for crack propagation throughout the HMAC layer, N_p, characterize the fatigue resistance of HMAC.

Crack initiation is the first stage of fracture process in HMAC. During this stage, microcracks will grow and join together to form macrocracks. When the length of macrocracks reaches 7.5 mm, cracks will propagate through the HMAC layer.

The number of loading cycles to crack initiation, N_i, is related to the rate of DPSE increase (b), crack density (C_D), Paris Law fracture coefficients (A and n), through the Equation 1-8.

$$N_i = \frac{C_{\max}^{1+2n}}{A}\left(\frac{4\pi A_c}{b}\right)^n C_D^n \tag{1-8}$$

where $C_{\max}$ is the maximum length of microcrack, or the initial length of macrocrack before crack propagation. The threshold value that defines the end of crack initiation and start of crack propagation is taken as 7.5 mm from Lytton et al.'s data (*5*). C_D, crack density, is the number of cracks per unit area. A value of 2.317 mm^{-2} was used in project 0-4468. A_c is cross-sectional area of the mixture specimen. In project 0-4468, the specimen has a diameter of 4 inches. b is the rate of increase of DPSE. It is determined

from relaxation modulus (RM) test in tension and repeated direct tension (RDT) test[1]. A and n are Paris Law fracture coefficients. They are determined from tensile strength test (TS), RM test, and surface energy (SE) measurements of aggregate and binder.

For the CMSE method as implemented in project 0-4468, Equation 1-8 can be simplified by substituting numerical values:

$$N_i = \frac{0.0075^{1+2n}}{A}\left(\frac{2.366\times10^5}{b}\right)^n \tag{1-9}$$

A and n can be calculated from Equations 1-10 and 1-11:

$$A = 0.165\sigma_t^{-2}\frac{E_t^m}{\Delta G_f}\left(\frac{\sin(m\pi)}{m\pi}\right)^{1-m}[0.5042 - 0.1744\ln(n)] \tag{1-10}$$

$$n = \frac{1}{m} \tag{1-11}$$

where E_t and m are relaxation modulus and rate of stress relaxation from RM test, and σ_t is tensile strength from TS test, and ΔG_f is fracture surface energy obtained from surface energy measurement.

The above three equations are implemented in fatigue analysis software developed in Chapter IV, for crack initiation calculation. Because these equations are derived for test results from TxDOT project 0-4688, it is important that mixture tests follow exactly the protocols specified in that project.

Following the formation of macrocracks in crack initiation, cracks with length of

[1] Detailed specifications of RM and RDT tests, as well as other mixture tests (tensile strength test, surface energy test) can be found in TxDOT project 4468. Because this thesis is focused on software development, only the basic theories and equations are described herein.

7.5 mm or greater will propagate in the HMAC layer. The number of loading cycles for macrocracks to spread throughout HMAC layer, N_p, is a function of the HMAC layer thickness, mixture shear modulus, Paris Law fracture coefficients, and design shear strain.

$$N_p = \frac{d^{1-\frac{n}{2}}}{A \cdot (2r \cdot S \cdot G)^n (1 - n \cdot q)} \frac{1}{\gamma^n} \left(1 - \frac{C_{\max}}{d}\right)^{1-n \cdot q} \quad (1\text{-}12)$$

$$S = \frac{1-\nu}{1-2\nu} \quad (1\text{-}13)$$

$$G = \frac{E_t}{2(1+\nu)} \quad (1\text{-}14)$$

In Equation 1-12, A and n are fracture coefficients, $C_{\max}$ is maximum microcrack length, as defined in previous section. d is the thickness of HMAC layer. r and q are regression constants for the stress intensity factor. According to Lytton et al. (*5*), r = 4.397, and q = 1.18. The shear modulus coefficient, S, is a function of Poisson's ratio ν. G is the mixture shear modulus. γ is maximum design shear strain. It depends on traffic loading, pavement structure, and material properties. Stress-strain analysis software could be used to obtain the design shear strain.

Substituting Equations 1-13 and 1-14 and other values into Equation 1-12 gives

$$N_p = \frac{d^{1-\frac{n}{2}}}{A \cdot \left[4.397 E_t \frac{1-\nu}{(1+\nu)(1-2\nu)}\right]^n (1 - 1.18n)} \frac{1}{\gamma^n} \left(1 - \frac{0.0075}{d}\right)^{1-1.18n} \quad (1\text{-}15)$$

This equation is implemented in fatigue analysis software to account for mixture fatigue life during crack propagation.

The sum of N_i and N_p gives the fatigue life of a mixture as measured in the laboratory. For field mixtures, further analysis is complicated by several factors. The most important factors are aging, healing, and anisotropy of the mixture.

The effect of healing and anisotropy are taken into account by shifting factors SF_h and SF_{an}. Based on the findings in project 0-4468, a value of 2.0 is used for SF_{an}. SF_h can be calculated using Equation 1-16:

$$SF_h = 1 + g_5\left(\frac{\Delta t_r}{a_{TSF}}\right)^{g_6} \tag{1-16}$$

g_5 and g_6 are field calibration factors, which values can be found in TxDOT project 0-4468; a_{TSF} is temperature shifting factor used to adjust results from laboratory temperature to field temperature; Δt_r is rest period between major traffic loading cycles.

With shifting factors, field fatigue life is calculated from Equation 1-17:

$$N_f = SF_{an} \cdot SF_h \cdot (N_i + N_p) \tag{1-17}$$

Note, the effect of aging is not included yet. Due to its complexity, it will be discussed separately in the following section.

Binder aging in mixtures has great impact on mixture fatigue resistance because it changes several fundamental properties of both binders and mixtures. According to the study in TxDOT project 0-4468, with binder aging, the fracture surface energy of binder will decrease and the healing surface energy of binder will increase, which in turn results in lower fracture energy and higher healing energy for the mixture. As a result, the mixture is easier to fracture but harder to self-heal. Aging also makes the mixture stiffer, so that it has a higher relaxation modulus and smaller stress relaxation rate. In addition,

the rate of increase of DPSE, or the rate of damage accumulation, also increases with binder aging. All these deteriorations in binder and mixture properties lead to a decline of fatigue resistance.

In the second and third phase of project 0-4468 (*17, 18*), the effect of binder aging on mixture fatigue performance was evaluated. It was found that the DSR Function of a binder might have good correlation with mixture fatigue life. A similar conclusion is also drawn in TxDOT project 0-4688 (*19*). Figure 1-3 shows the decline of pavement fatigue life with binder aging in terms of the DSR function. It seems a linear relationship might exist from this log-log scale plot.

By assuming the linear relationship between log binder DSR function and log fatigue life, the decline of fatigue life with binder aging can be predicted using:

$$K_1 = \frac{d\ln(N_f)}{d\ln(DSR_{fn})} \tag{1-18}$$

where K_1 is the slope of N_f decline with DSR function in log-log scale and can be measured in laboratory.

Fatigue life of unaged mixture N_{f0} and DSR function of unaged binder DSR_{fn0} also can be measured. In addition, DSR function of binder in mixture can be estimated using binder aging model mentioned earlier. By integrating Equation 1-18, mixture field fatigue life at any time point can be calculated from

$$\ln\left(\frac{N_f}{N_{f0}}\right) = K_1 \ln\left(\frac{DSR_{fn}}{DSR_{fn0}}\right) \tag{1-19}$$

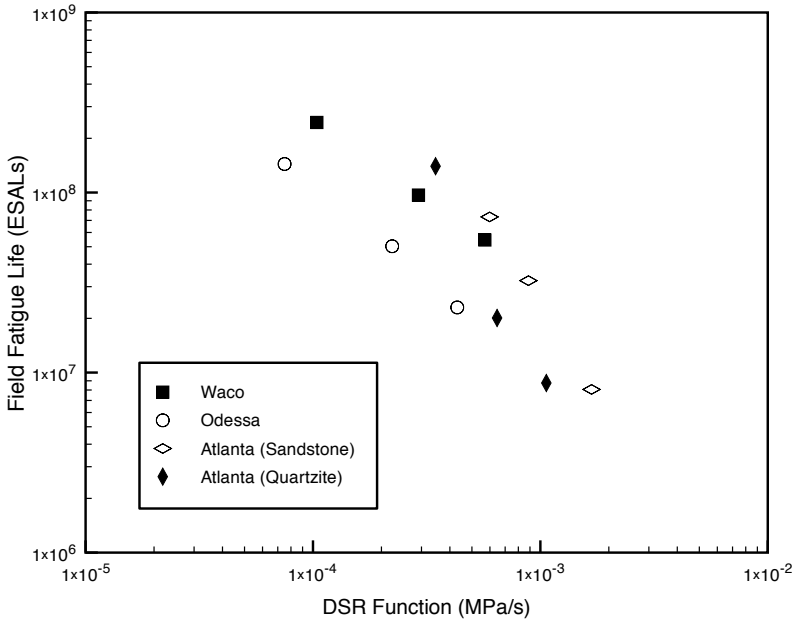

FIGURE 1-3 Pavement fatigue life decline with binder aging in terms of DSR function (data adapted from TxDOT project 0-4688).

Thesis Outline

The thesis outline is listed as following:

1. Experiment is designed for the study of fast-rate period binder oxidation and results are analyzed in Chapter II;
2. A new pattern-based hourly air temperature model is developed in Chapter III, and results are compared with conventional sinusoidal model;
3. The development and application of software for pavement aging and fatigue analysis will be in Chapter IV;
4. A collection of supplement data, which facilitates the application of software, is organized in Chapter V;
5. Conclusion and plan of future work are in Chapter VI.

CHAPTER II

STUDY OF EARLY FAST-RATE PERIOD OF BINDER OXIDATION

The early fast-rate period of binder oxidation is studied and preliminary results are presented and discussed in this chapter. This is the first endeavor to model fast-rate binder oxidation in terms of carbonyl formation.

Introduction

Early fast-rate oxidation of binder has been long observed in laboratory aging experiments. As early as 1959, Van Oort (*20*) had studied the oxygen absorption and viscosity change with time of several binders aging at room temperature and atmospheric pressure. Oxygen absorption and formation of carbonyl area show a fast increase at early times, and then the rates of change decreased to slower, constant rates at later times.

In reality, fast-rate oxidation begins at hot mix plant production to pavement laydown and ends in the early period of service. The duration of fast-rate period is assumed to be short, comparing to the much longer constant-rate period. Thus, researchers tend to believe that the fast-rate period is not as important as the constant-rate period, especially in terms of long-term binder performance. However, carbonyl area data of recovered binder from Texas Highway SH 21 field core (*9*) show that carbonyl formation during fast-rate period is roughly equivalent to four years of constant-rate aging in the field. That is about 20 percent contribution to binder field aging assuming a pavement design life of 20 years.

To simulate fast-rate oxidation in the laboratory, neat binder is usually aged using one of the short-term aging methods, the thin film oven test (TFOT), the rolling thin film oven test (RTFOT), or the stirred air flow test (SAFT). Then it is further aged and studied for constant-rate reaction kinetics and other properties, assuming that the fast-rate period has been passed.

While it is easier to tell whether or not the fast-rate period has been passed in the laboratory, it is more difficult to tell when it ends in the field. Mainly, this is due to the lower and cyclical field temperatures in pavements, especially those in cold climate regions. Another factor is the lower accessibility of air to binders in mixtures. Using constant-rate reaction kinetics to assess field aging without knowing if the fast-rate period has been passed may contribute considerable error and uncertainty to the results and conclusions. Thus, an improved understanding of oxidation kinetics during the fast-rate period is important, especially for prediction of the binder aging level in pavements and for other aging related properties.

In TxDOT project 0-4688 (*19*), recovered binders of field cores from Texas and Minnesota (MnRoad) were measured for rheological properties, and then aged further in a 60 °C environmental room (ER) for up to eight months. Figure 2-1 shows the stiffness (in the form of the DSR function) of each recovered binders (zero months), plus increases that occur with further ER aging (2, 4, 6, and 8 months). If the measured DSR functions form a single straight line, then the binder had past the fast-rate period in the field. However, if the binder, as recovered from the core, lies below a straight line formed by its subsequently-aged samples, then the core sample was still in the fast-rate

period. From Figure 2-1, it seems clear that the binder recovered from the Texas pavements had past the fast-rate period after two to three years aging in the pavement, whereas the MnRoad AC 120/150 binder was still within this period, even after 12 years of field aging. And it seems that the fast-rate period of aging is quite important for MnRoad in light of long-term pavement aging.

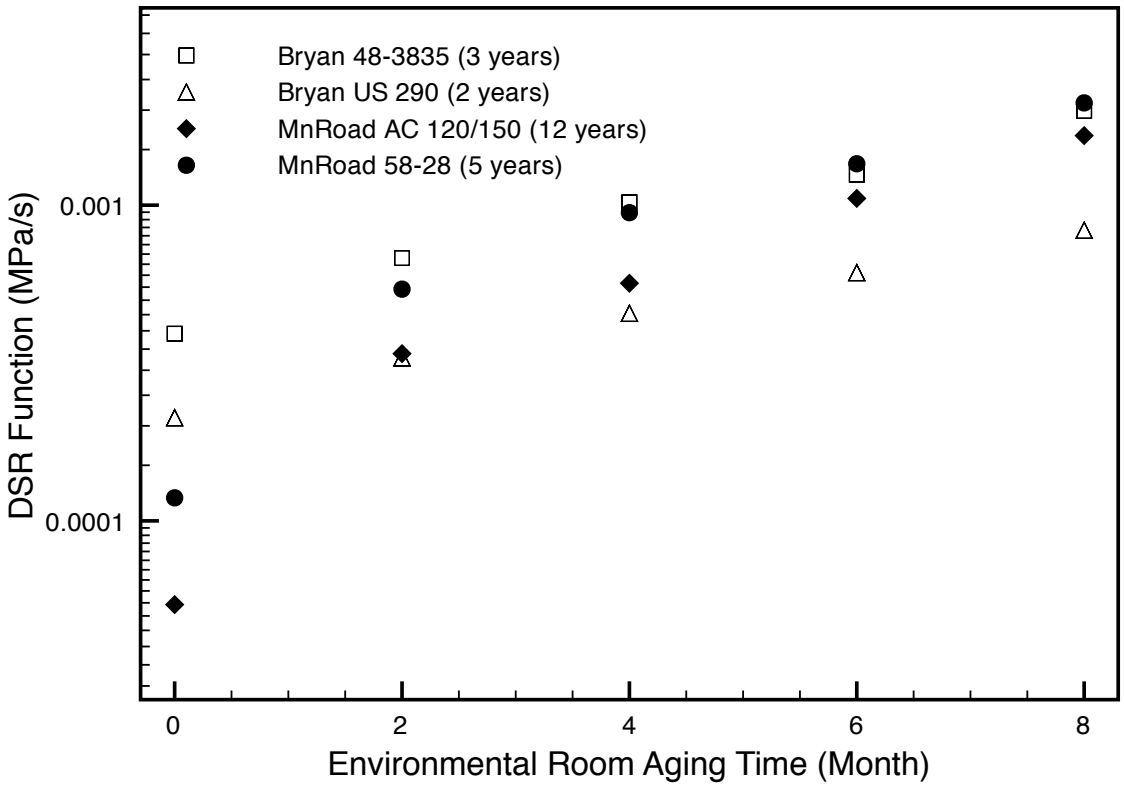

FIGURE 2-1 DSR function growth of recovered binders from Texas and Minnesota pavement aged in environmental room at 60 °C (data adapted from TxDOT project 0-4688).

Literature Review

About six decades ago, Dickenson and Nicholas (*21*) investigated the reaction of oxygen with tar oils at constant temperature and oxygen pressure. Two parallel reactions were suggested, one, a first order reaction with respect to phenol and the other, zero order reaction with respect to aromatics. The combined effect of these two reactions yielded a fast-rate period of oxygen absorption at the beginning, followed by a constant-rate period after the limiting reactant phenol depleted in first order reaction.

The proposed reaction kinetics for tar oil is as follows:

$$P = M(1 - e^{-k_2 t}) + kt \tag{2-1}$$

where P is the total amount of oxygen absorbed by tar oil, k and k_2 are reaction constants for the zero order reaction and first order reaction, respectively, M is the maximum oxygen absorption due to the first reaction.

The effects of temperature and oxygen pressure on oxidation were also examined. For all three oils studied, k and k_2 increased with temperature. Interestingly, M also increased with temperature. In addition, k and M increased with oxygen pressure, but k_2 did not vary significantly.

Researchers found that the viscosity of asphalt binders changes with aging in a similar way. In 1998, Herrington (*22*) aged several types of binders at constant temperatures (50, 60 and 70 °C) and 300 psi (about 20 atm) air pressure. Viscosities at 60 °C were measured at different aging times. The change of logarithmic viscosity fits the proposed two-reaction model very well. Kinetics parameters k and k_2 for change of logarithmic viscosity were obtained for two types of binder S180 and I180. These data

are taken from Herrington's paper to study the activation energy E_a and frequency factor A in the Arrhenius equation, as shown in Figures 2-2 and 2-3. Because the change of logarithmic viscosity shows a linear relationship with carbonyl area growth, it seems the same model should also fit carbonyl area data.

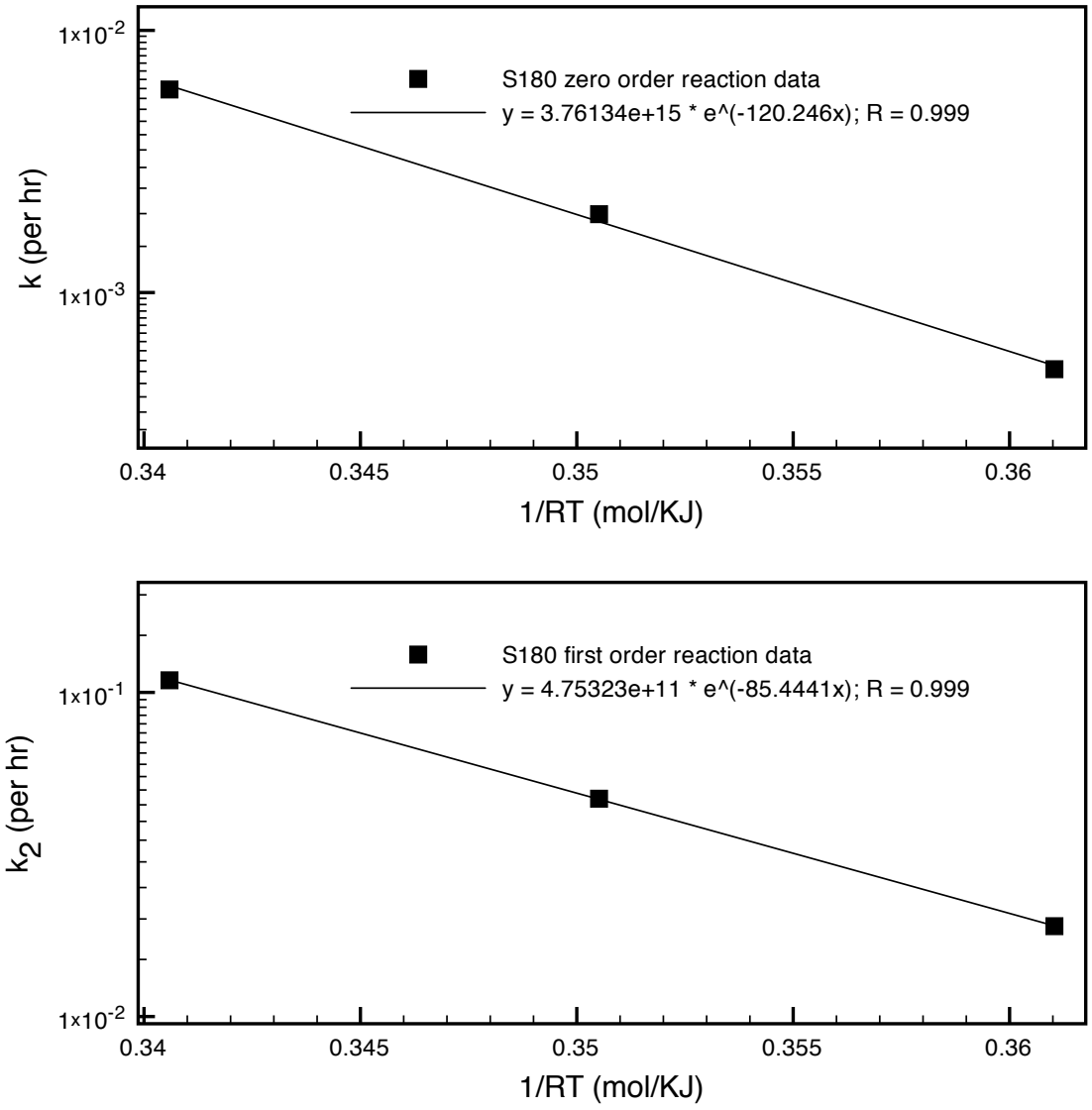

FIGURE 2-2 Activation energy E_a and pre-exponential factor A for S180 (data adapted from Herrington).

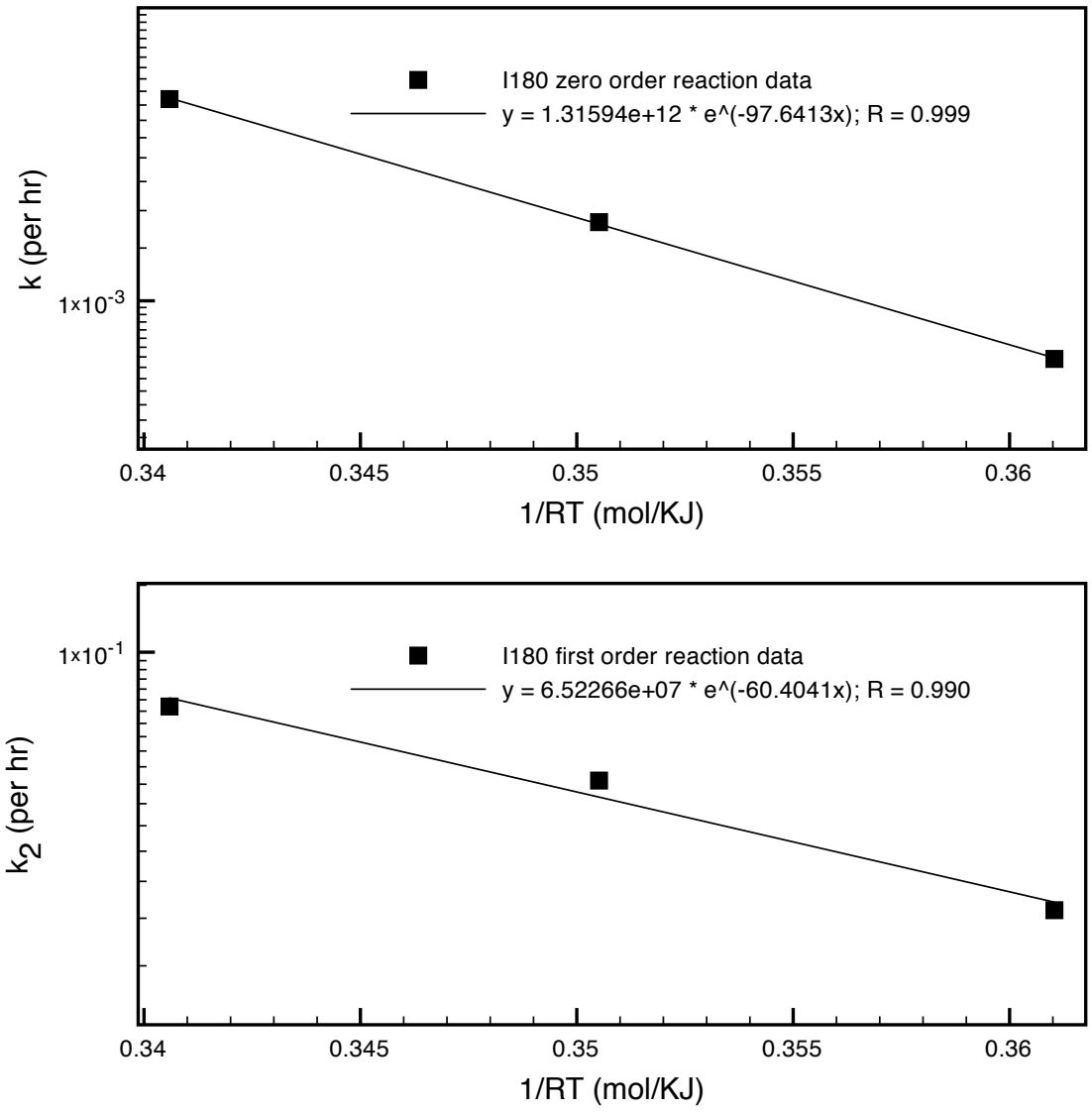

FIGURE 2-3 Activation energy E_a and pre-exponential factor A for I180 (data adapted from Herrington).

Some studies on binder aging characterize the fast-rate period with an initial jump, which is the intercept of constant-rate reaction line of carbonyl area formation (*3, 8, 9, 14*). The difference of initial jump and initial carbonyl area is thus the limiting formation of carbonyl area from first order reaction in the two-reaction model. Liu et al.

(*3*) found, based on a study of 15 asphalts, that the initial jump is not a function of temperature, but rather is a function of oxygen pressure.

Experimental Design

Two asphalts were used in this study of binder reaction kinetics: SEM 64-22 (unmodified) and SEM 70-22 (SBS-modified). About 2.4 grams of asphalt of each type was put into 4 cm by 7 cm aluminum trays to form an approximately 1 mm thin film. A thin film was used to reduce the effect of oxygen diffusion on binder aging.

The trays of binder were placed in five pressure oxygen vessels (POVs) at five temperatures (*23*). The POVs are immersed in a triethylene glycol (TEG) bath with the temperature controlled at a constant set point. The POVs are also purged by preheated air to insure adequate oxygen supply at atmospheric pressure.

For each asphalt type, two to three trays were retrieved from the POV according to Table 2-1. Each sample was analyzed using a Thermo Scientific Nicolet 6700 FT-IR. Carbonyl area was measured as the absorbance peak area from 1650 to 1820 cm^{-1}. Two to three data points were obtained, and an average value was used.

TABLE 2-1 Aging Temperatures and Sampling Times

Aging Temperature (C)	Sampling Time (day)
62.8	1, 5, 10, 15, 20, 30, 45, 60, 74
68.4	1, 3, 5, 7, 10, 15, 20, 25, 30 41, 50
78.2	1, 3, 5, 7, 10, 15, 20, 30, 40, 50, 60
87.0 and 97.7	1, 2, 4, 6, 10, 15, 20, 25, 30

Results and Discussion

Figures 2-4 and 2-5 show the increase of carbonyl area with time at five temperatures, for SEM 64-22 and SEM 70-22, respectively. From these two figures, a fast-rate period plus a constant-rate is clearly observed, especially at high temperatures.

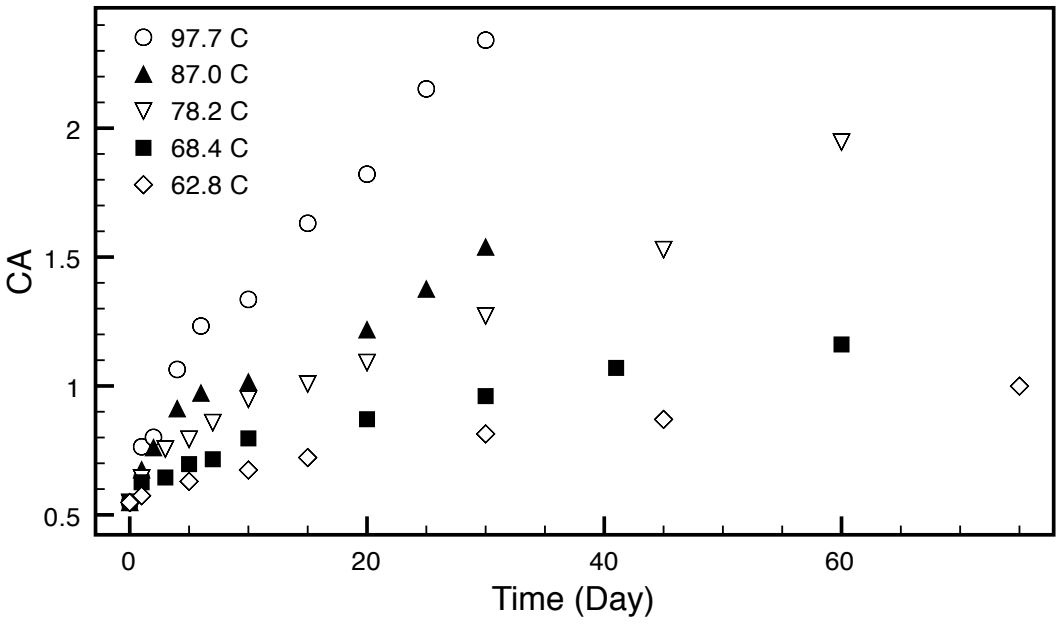

FIGURE 2-4 Carbonyl area growth with time for binder SEM 64-22 at five temperatures and atmospheric air pressure.

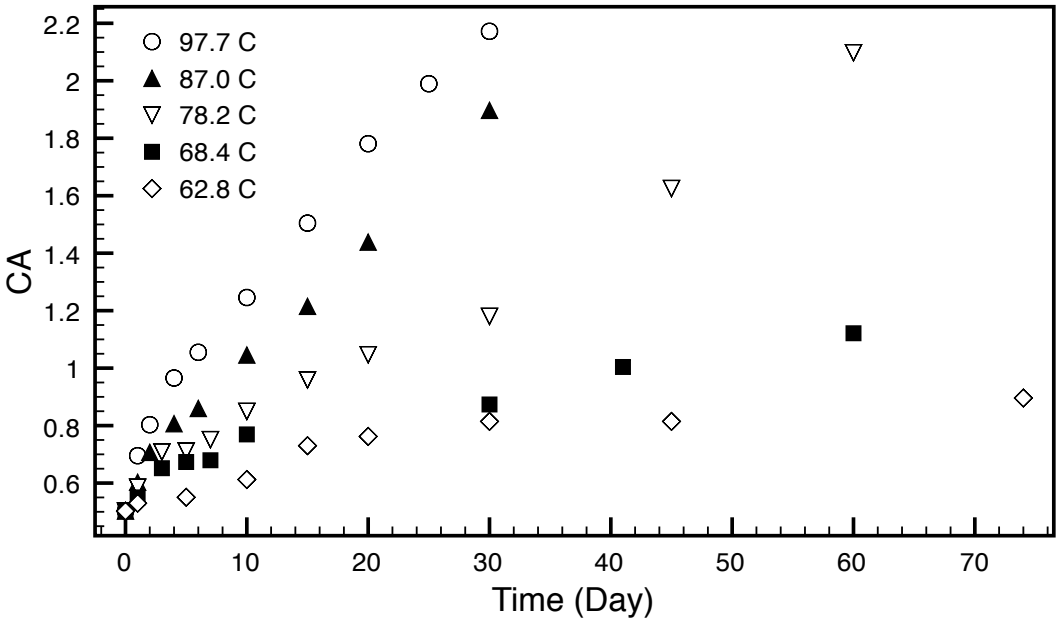

FIGURE 2-5 Carbonyl area growth with time for binder SEM 70-22 at five temperatures and atmospheric air pressure.

Based on the literature review and experimental data, the following hypothesis is proposed: carbonyl area is formed from two parallel reactions, one first order reaction and one zero order reaction with respect to some unknown species in asphalt. The formation of carbonyl area can be expressed in the following equation:

$$CA = CA_0 + (IJ - CA_0) \cdot (1 - e^{-k_f \cdot t}) + k_c \cdot t \qquad (2\text{-}2)$$

where CA is carbonyl area formed in asphalt, CA_0 is the initial carbonyl area of neat asphalt, IJ is initial jump, k_f and k_c are reaction constants for the first order reaction and the zero order constant-rate reaction, respectively. Figure 2-6 shows the hypothesis with initial jump (the grey horizontal line) and initial carbonyl area CA_0.

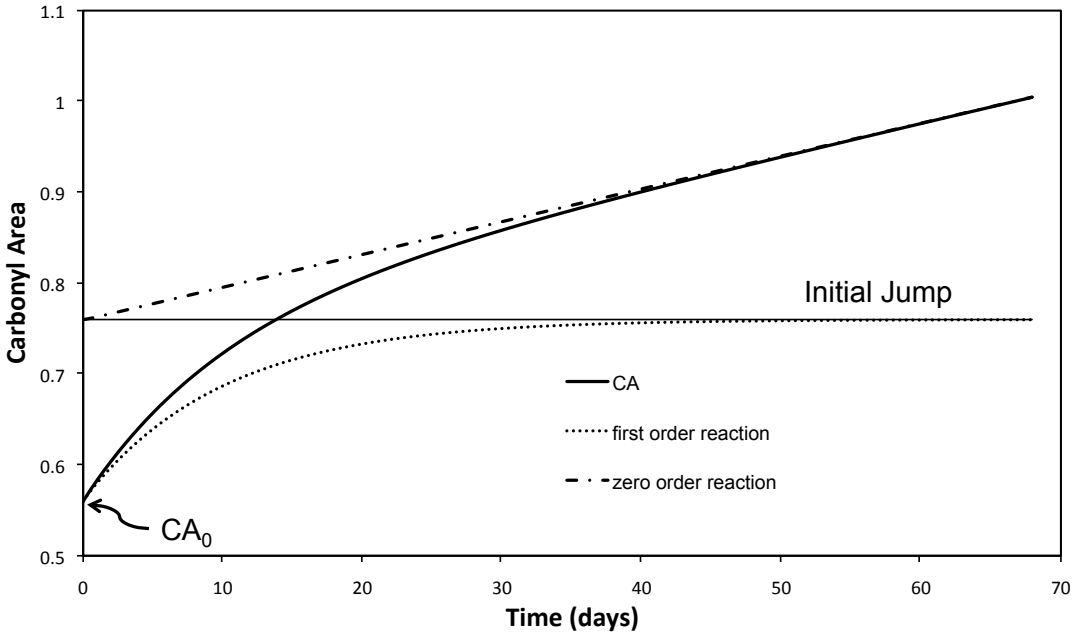

FIGURE 2-6 Two parallel reactions hypothesis of carbonyl area formation.

To test the hypothesis, data from the later period of aging are analyzed for the constant-rate reaction constant. Figures 2-7 and 2-8 show the effect of temperature on the constant-rate oxidation of SEM 64-22 and SEM 70-22. The slopes of the constant lines are reaction constants for zero order reaction, and the intercepts are initial jumps.

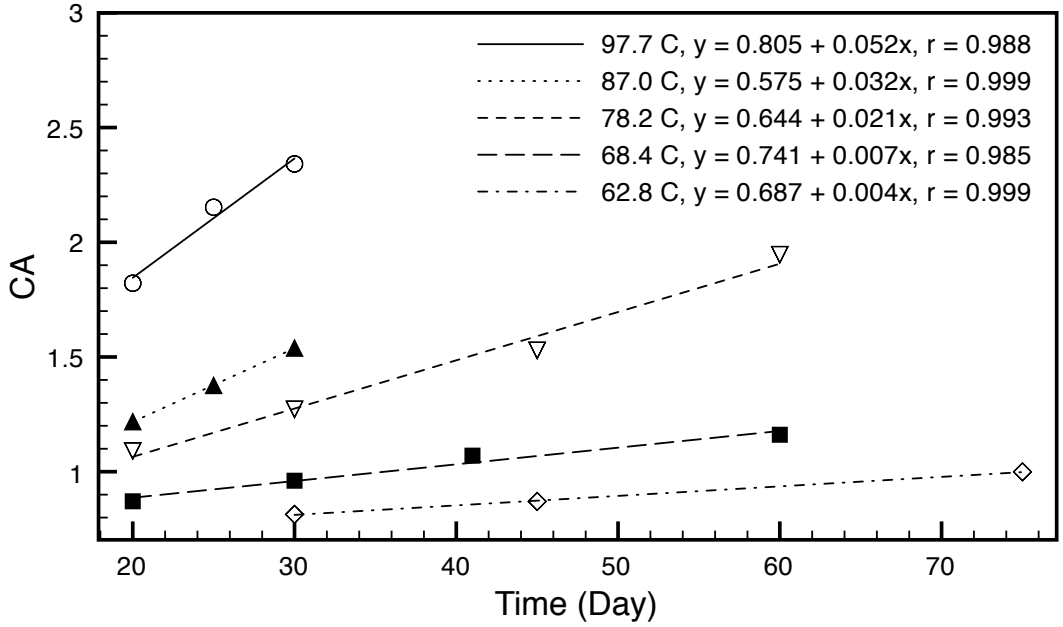

FIGURE 2-7 Effect of temperature on constant oxidation rate of SEM 64-22.

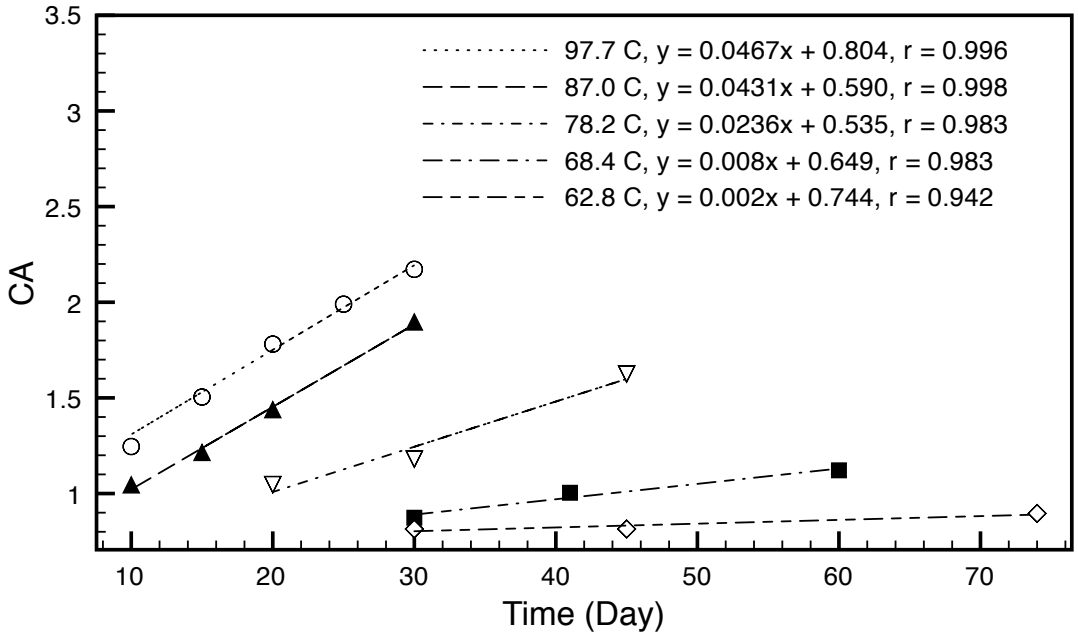

FIGURE 2-8 Effect of temperature on constant oxidation rate of SEM 70-22.

The constant-rate reaction constants k_c for five temperatures are then plotted versus *1/RT* in a semi-log scale, shown in Figures 2-9 and 2-10, to obtain activation energy E_a and pre-exponential factor A in Arrhenius equation:

$$k_c = A \cdot \exp(-\frac{E_a}{RT}) \tag{2-3}$$

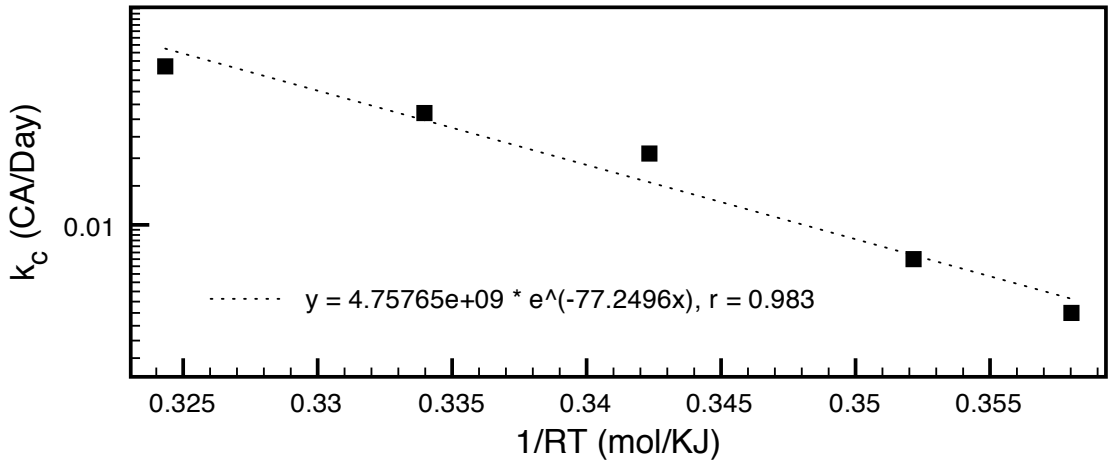

FIGURE 2-9 E_a and A of constant-rate reaction for SEM 64-22.

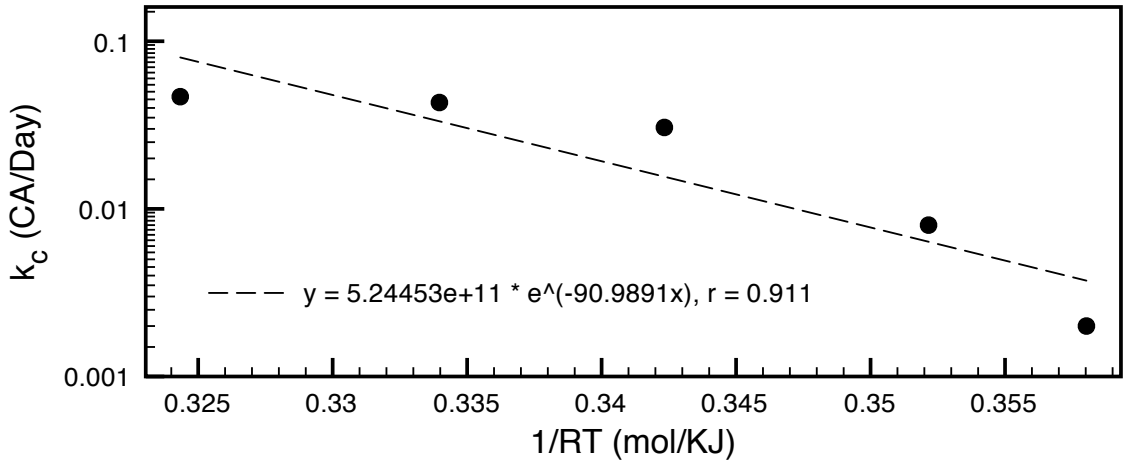

FIGURE 2-10 E_a and A of constant-rate reaction for SEM 70-22.

The hypothesis in Equation 2-2 states that the overall CA formation is the sum of CA_0 and CA formed in constant-rate reaction and in first-order reaction. Therefore, after subtraction of CA_0 and CA formed in constant-rate reaction from overall carbonyl area, CA formation following the first-order reaction in Equation 2-2 is expected. The CA data after subtraction are plotted in Figures 2-11 through 2-15.

Carbonyl area data of hypothetical first order reaction for SEM 64-22 show some support on the proposed two-reaction hypothesis, especially from data at three lower temperatures shown in Figures 2-11, 2-12, and 2-13. However, high-temperature data at 97.7 °C in Figure 2-14 has great variation, and 87.0 °C data in Figure 2-15 seems to suggest a different story.

Despite some discrepancies, the majority of data seems to support the hypothetical two-reaction kinetics model. From Figures 2-11 through 2-14, the first order reaction kinetics shown in Equation 2-4 is fitted with these data of SEM 64-22. Residual sum of square (RSS) values are also shown.

$$CA_f = M \cdot (1 - e^{-k_f \cdot t}) \tag{2-4}$$

where CA_f is formation of carbonyl area from first order reaction, $M = (IJ - CA_0)$.

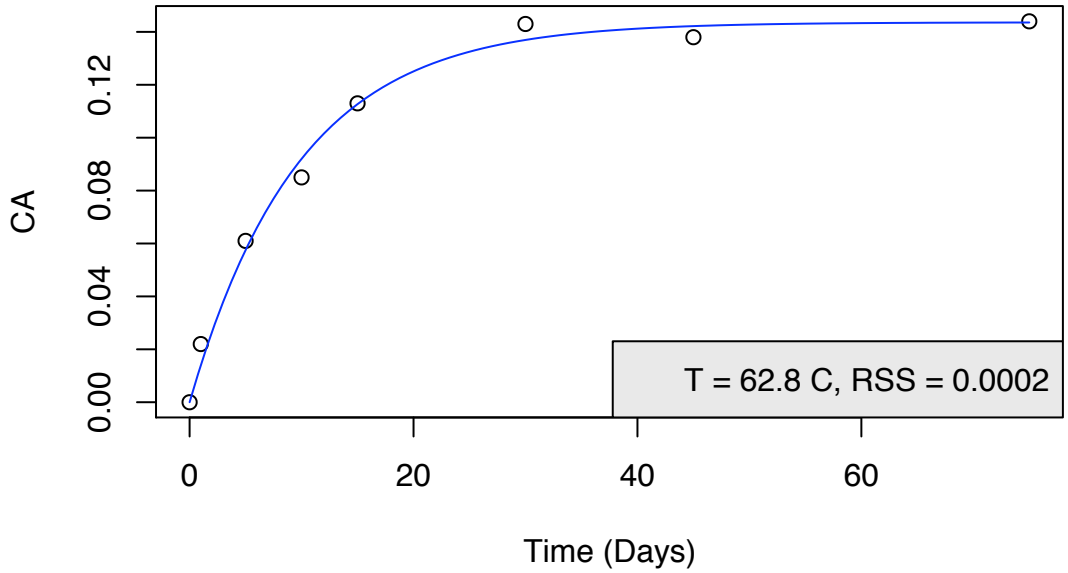

FIGURE 2-11 Nonlinear least square fit of hypothetical first order reaction data (62.8 °C) of SEM 64-22.

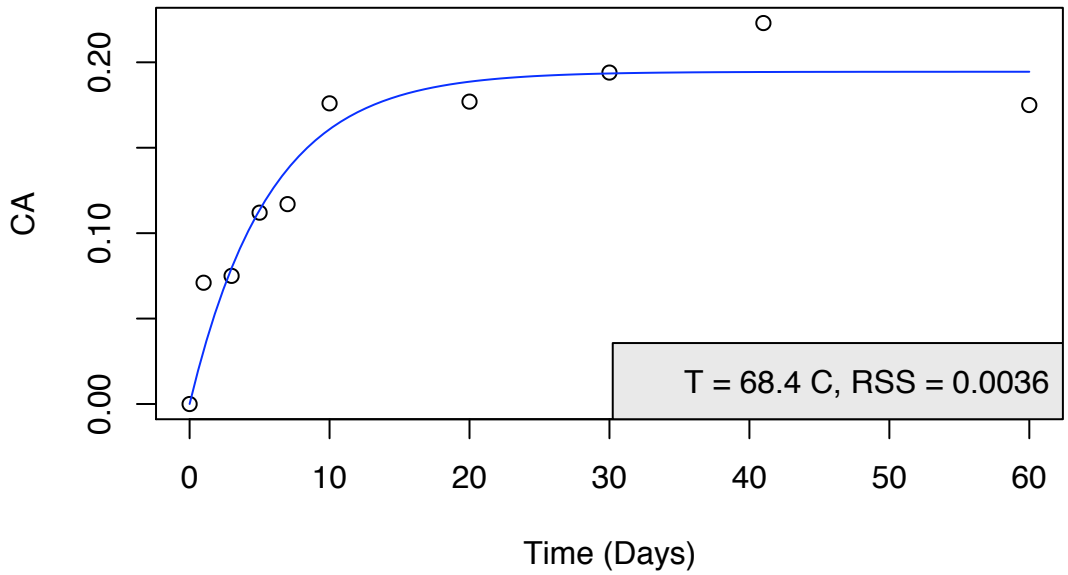

FIGURE 2-12 Nonlinear least square fit of hypothetical first order reaction data (68.4 °C) of SEM 64-22.

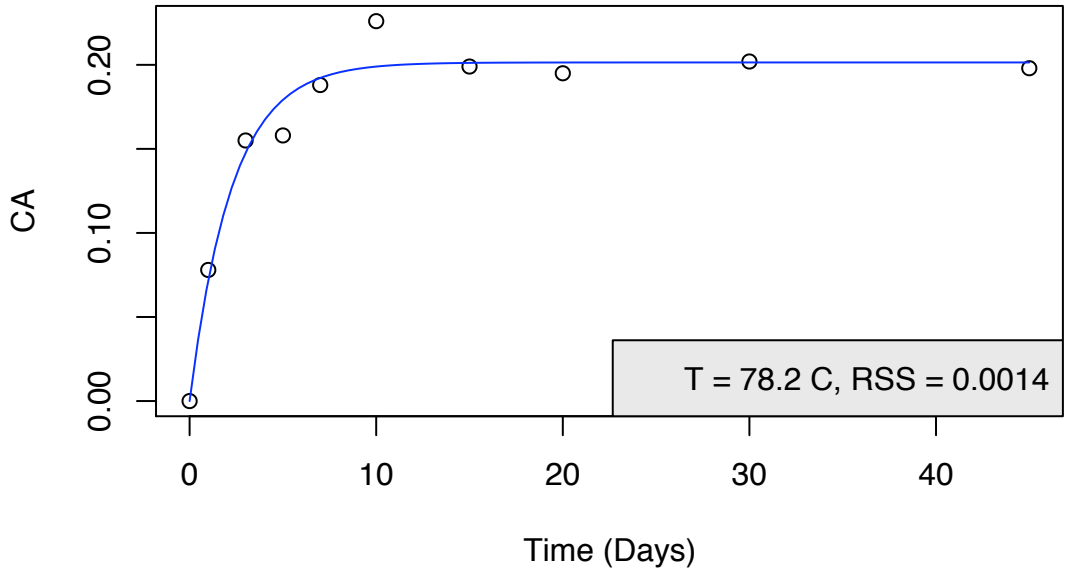

FIGURE 2-13 Nonlinear least square fit of hypothetical first order reaction data (78.2 °C) of SEM 64-22.

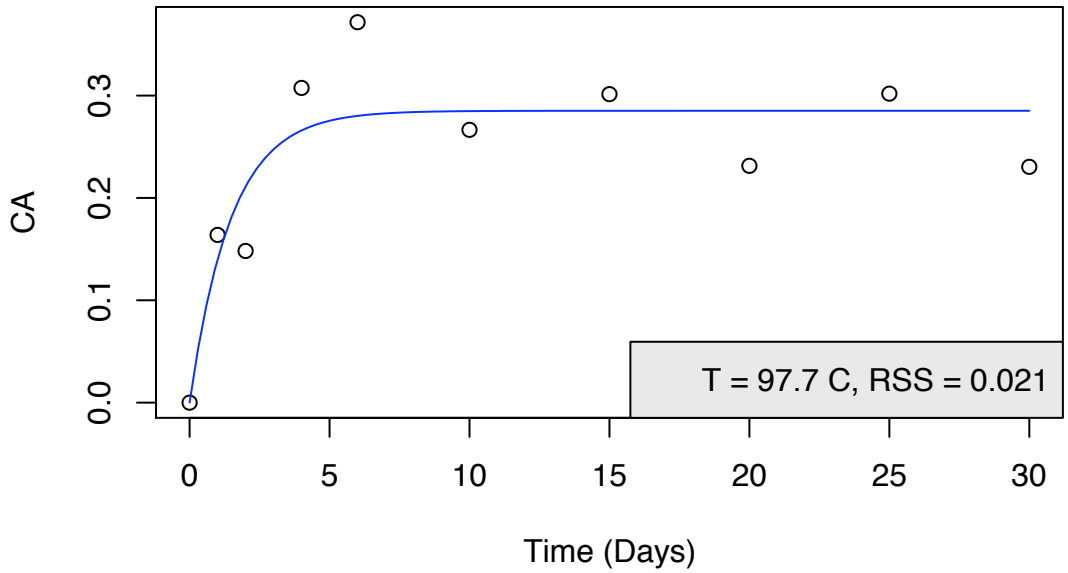

FIGURE 2-14 Nonlinear least square fit of hypothetical first order reaction data (97.7 °C) of SEM 64-22.

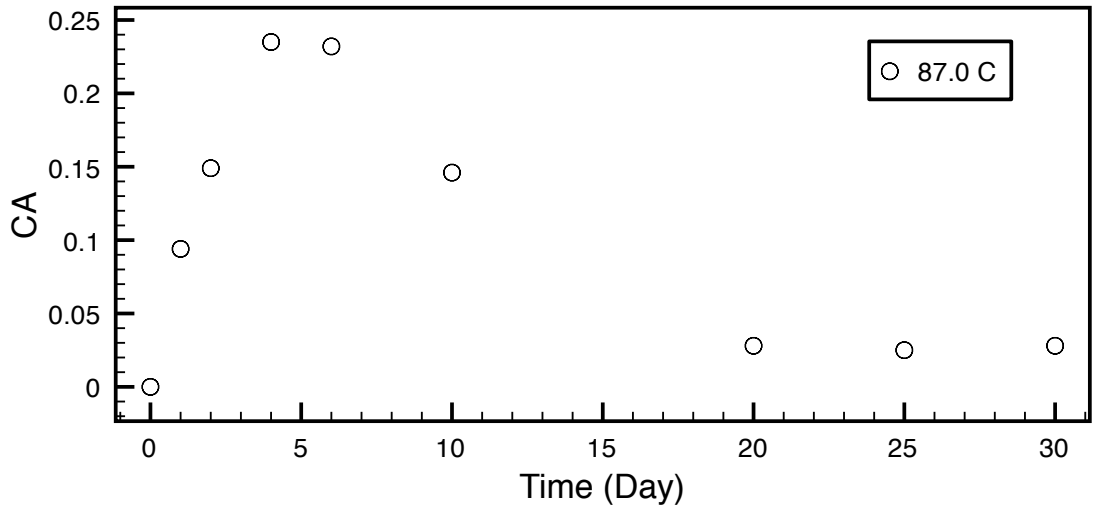

FIGURE 2-15 Hypothetical first order reaction data (87.0 °C) of SEM 64-22.

Table 2-2 summarizes *M* value and k_f from nonlinear least square estimation and k_c from previous constant-rate data. Note the RSS values for the three lower temperatures are small.

TABLE 2-2 M and Reaction Constants of SEM 64-22

Temperature (°C)	M	k_f	RSS	k_c
62.8	0.144	0.102	0.0002	0.004
68.4	0.194	0.175	0.0036	0.007
78.2	0.2014	0.441	0.0014	0.021
97.7	0.285	0.675	0.021	0.052

Figure 2-16 shows the activation energy and pre-exponential factor for the hypothetical first order reaction. The fit is fair. However, the Arrhenius equation fits the three low-temperature reaction constants extremely well (r = 1) as shown in Figure 2-16.

Figure 2-17 shows the M values. For SEM 64-22, M seems to increase with temperature, which agrees with data of tar oil (*21*) but does not agree with data of asphalt binder from Liu et al. (*3*).

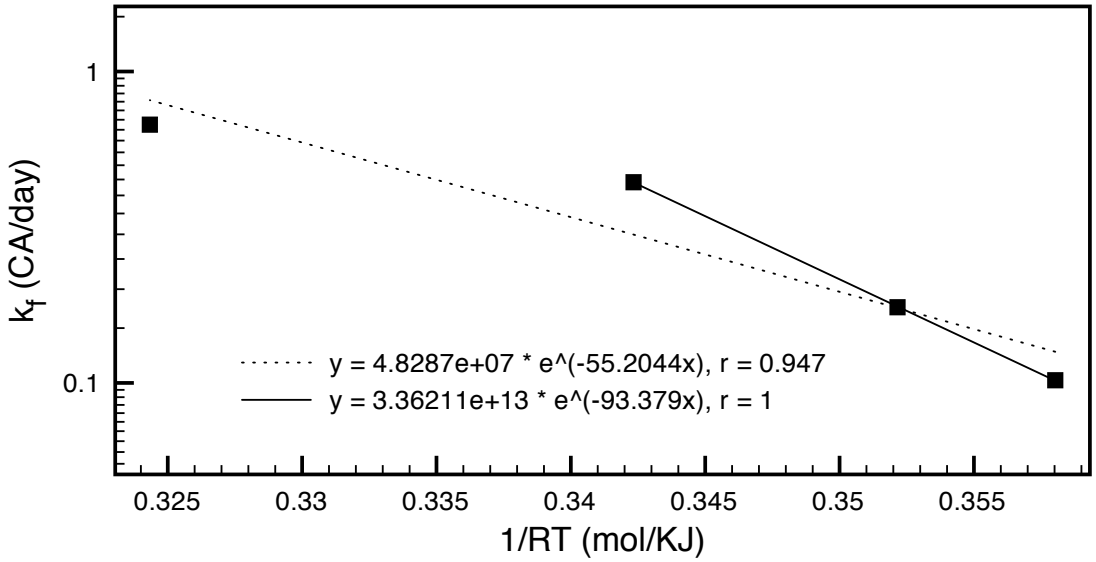

FIGURE 2-16 E_a and A for hypothetical first order reaction (SEM 64-22).

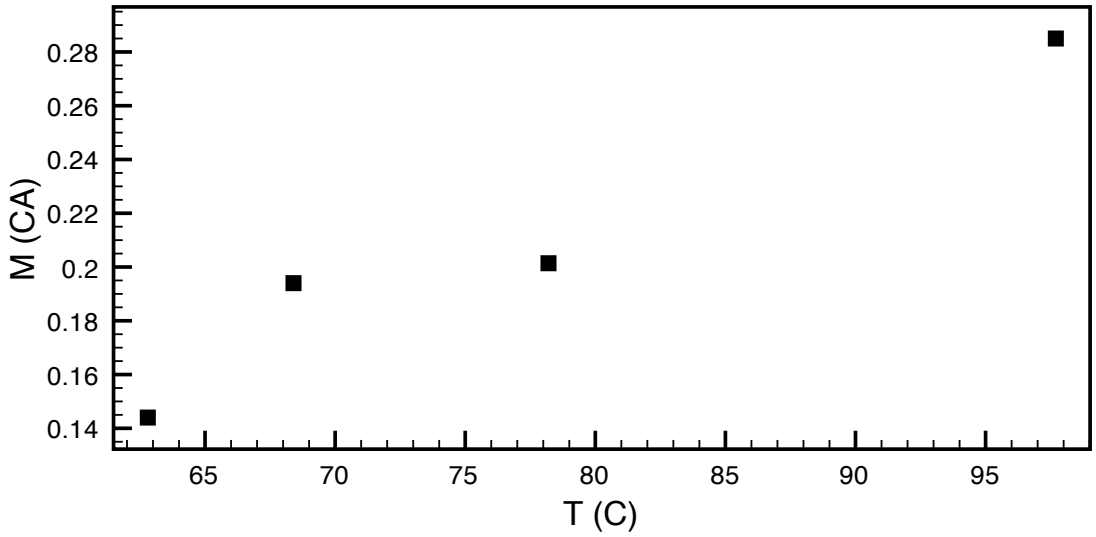

FIGURE 2-17 M value for hypothetical first order reaction (SEM 64-22).

Carbonyl area data for SEM 70-22 are shown in Figures 2-18 through 2-22. They also show support for the hypothesis, except data of 78.2 °C (Figure 2-21) after 30 days aging. Interestingly, data of 78.2 °C after 30 days aging shows an increasing trend, which is quite unexpected. Because the contribution from constant-rate reaction is subtracted before data are plotted, a close-to-horizontal line was expected. This discrepancy leads to a re-examination of constant-rate data at 78.2 °C in Figure 2-8. The r value for data at that temperature is 0.983, which means the goodness of fit is satisfactory but not perfect. Back to Figure 2-21, it seems reasonable to argue that, the irregularity of the hypothetical first order reaction data, to some extent, comes from the fitting of constant-rate data.

The same nonlinear least square regression is used for analysis of SEM 70-22 data. Nonlinear least square estimations are shown in Figures 2-18 through 2-20. Nonlinear least square regression is not successful for data of 78.2 and 87.0 °C, because the model does not fit those data.

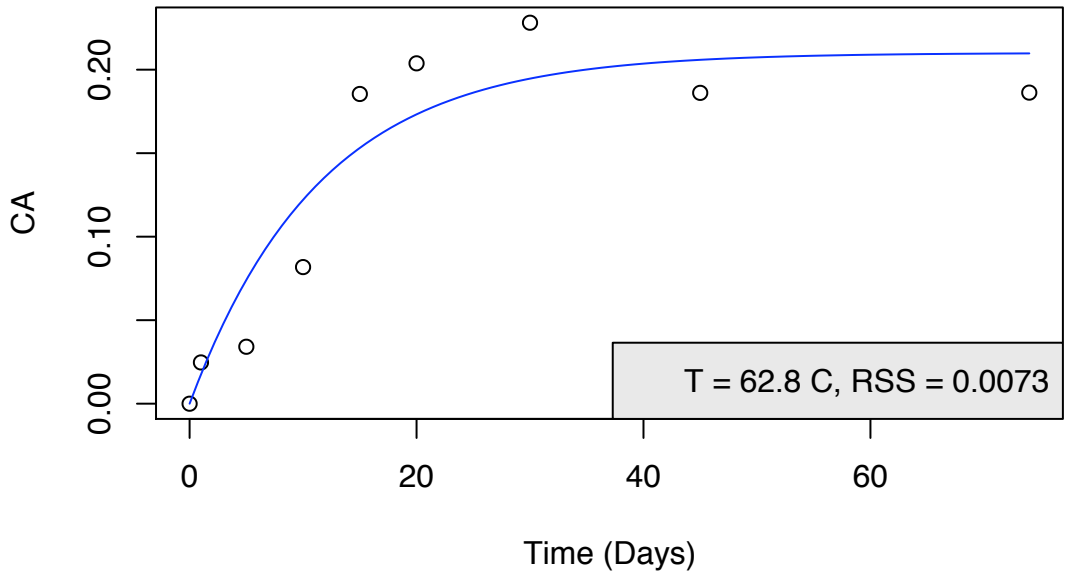

FIGURE 2-18 Nonlinear least square fit of hypothetical first order reaction data (62.8 °C) of SEM 70-22.

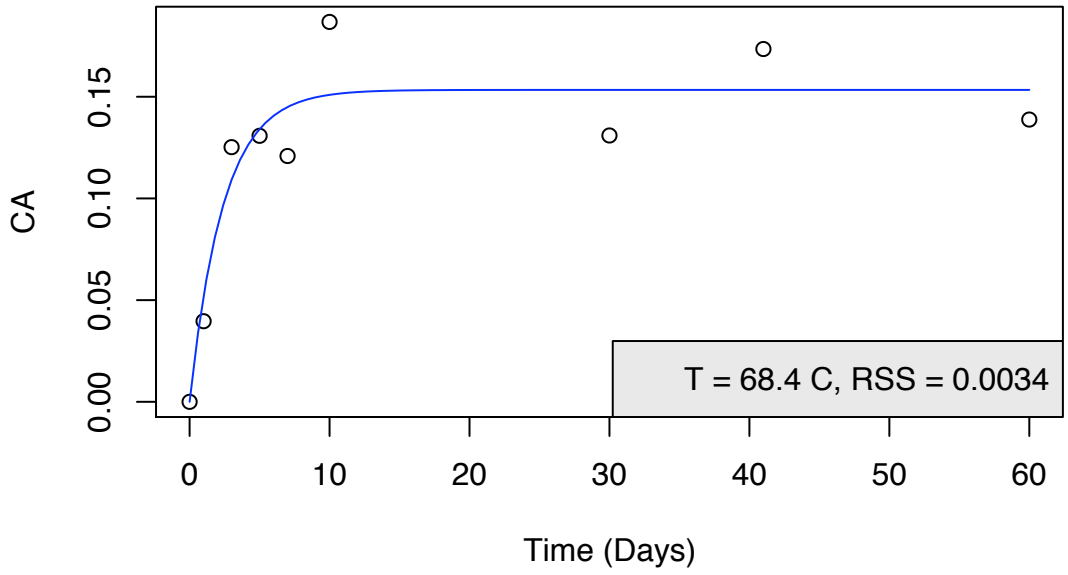

FIGURE 2-19 Nonlinear least square fit of hypothetical first order reaction data (68.4 °C) of SEM 70-22.

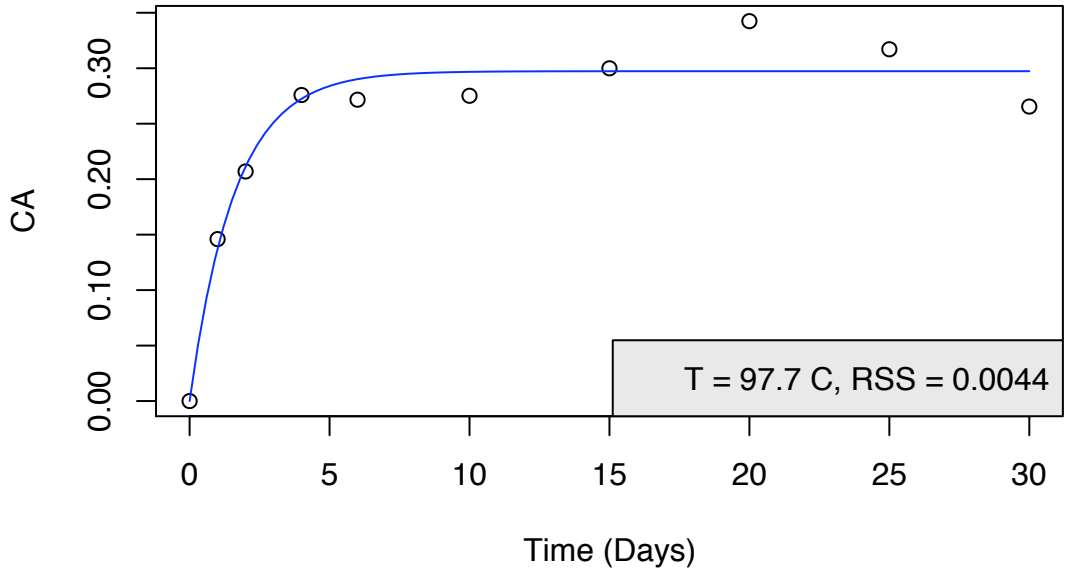

FIGURE 2-20 Nonlinear least square fit of hypothetical first order reaction data (97.7 °C) of SEM 70-22.

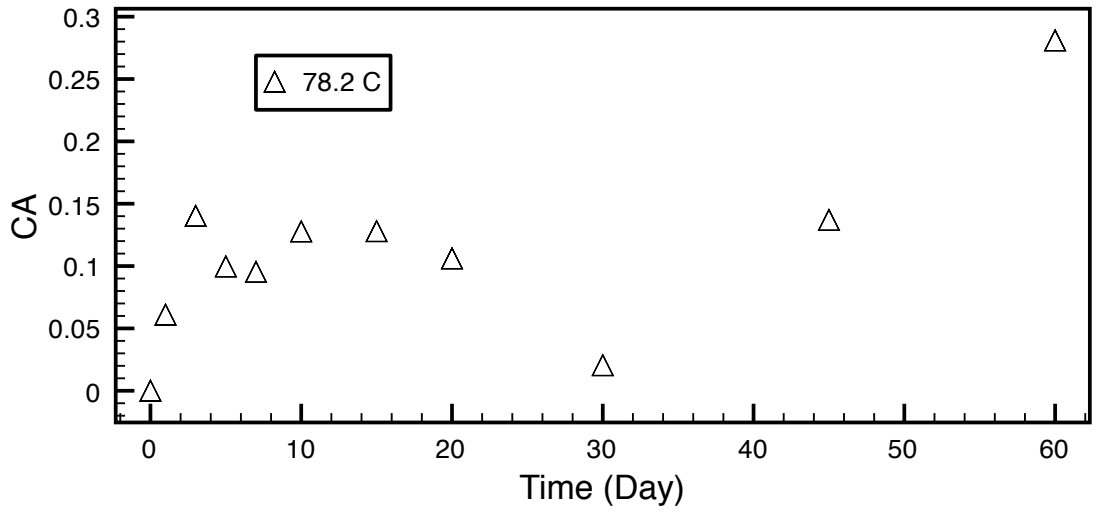

FIGURE 2-21 Hypothetical first order reaction data (78.2 °C) of SEM 70-22.

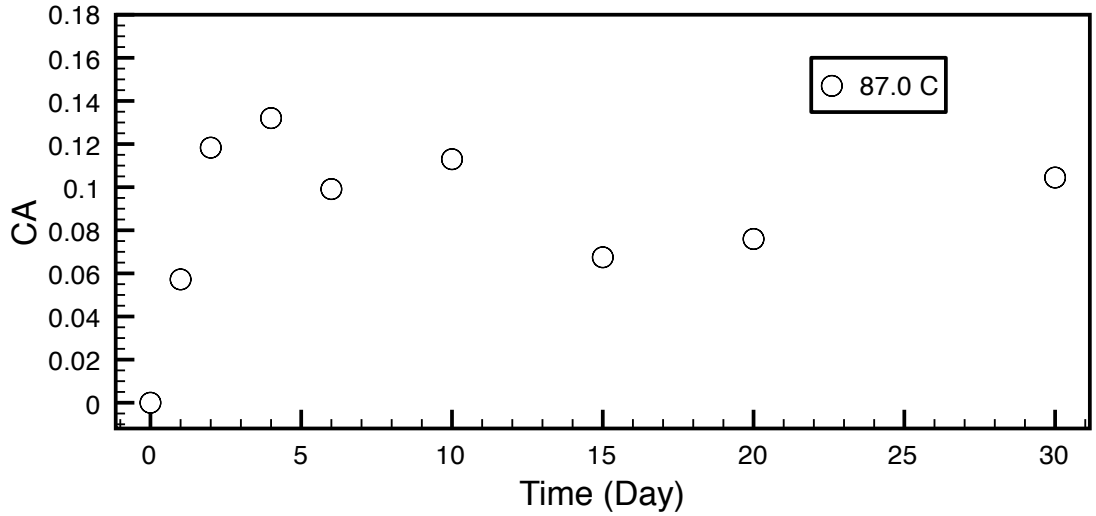

FIGURE 2-22 Hypothetical first order reaction data (87.0 °C) of SEM 70-22.

M values and reaction constants obtained are listed in Table 2-3. Figure 2-23 shows activation energy and pre-exponential factor for SEM 70-22. Figure 2-24 plots the effect of temperature on M.

TABLE 2-3 M and Reaction Constants of SEM 70-22

Temperature (°C)	M	k_f	RSS	k_c
62.8	0.2101	0.0871	0.0073	0.002
68.4	0.1534	0.4149	0.0034	0.008
97.7	0.2973	0.6208	0.0044	0.0467

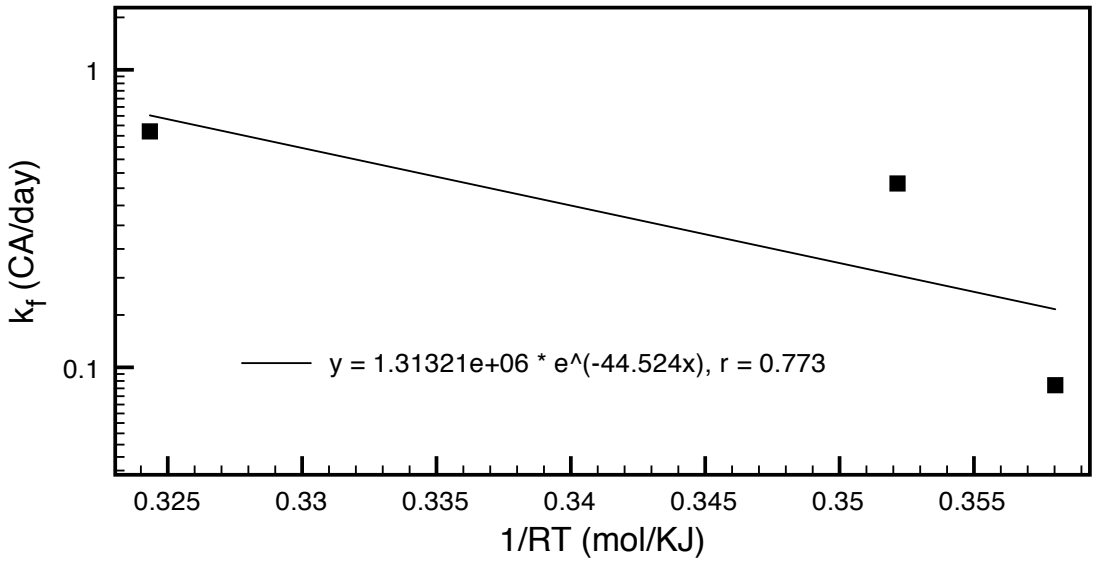

FIGURE 2-23 E_a and A for hypothetical first order reaction (SEM 70-22).

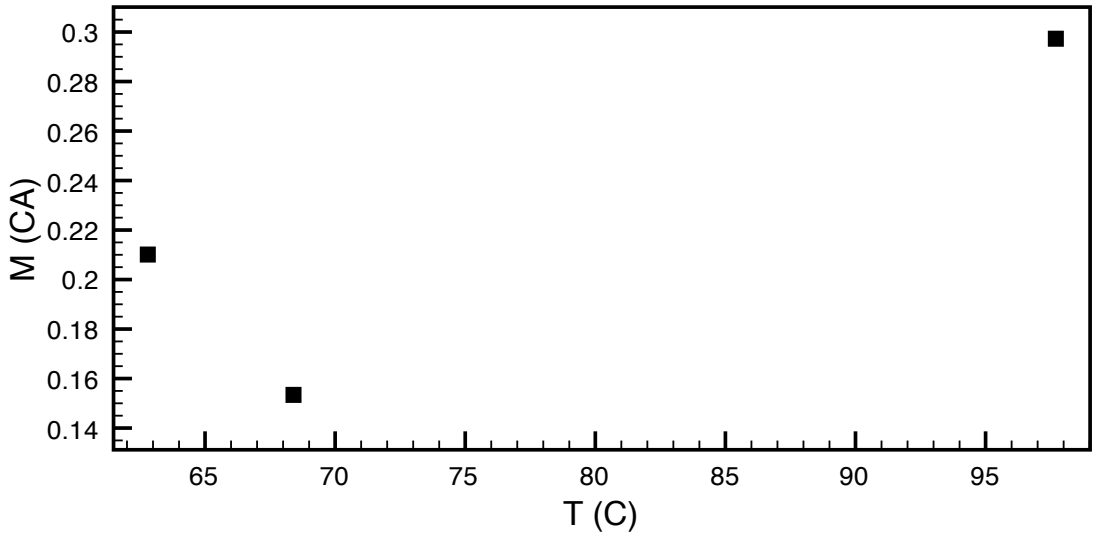

FIGURE 2-24 M value for hypothetical first order reaction (SEM 70-22).

To alleviate the irregularity of data introduced by fitting of constant-rate data, instead of estimate parameters for two reactions individually, original carbonyl area data

are analyzed using nonlinear least square estimation to obtain parameters for both reactions.

Nonlinear least square fitting for SEM 64-22 is shown in Figure 2-25. Parameter estimations are tabulated in Table 2-4. Activation energy and pre-exponential factor for constant-rate and first order reaction are shown in Figures 2-26 and 2-27. Again, reaction constant for both constant-rate reaction and first-order reaction are shown for the three low temperatures. The goodness of fit is also exceptional. M values are shown in Figure 2-28.

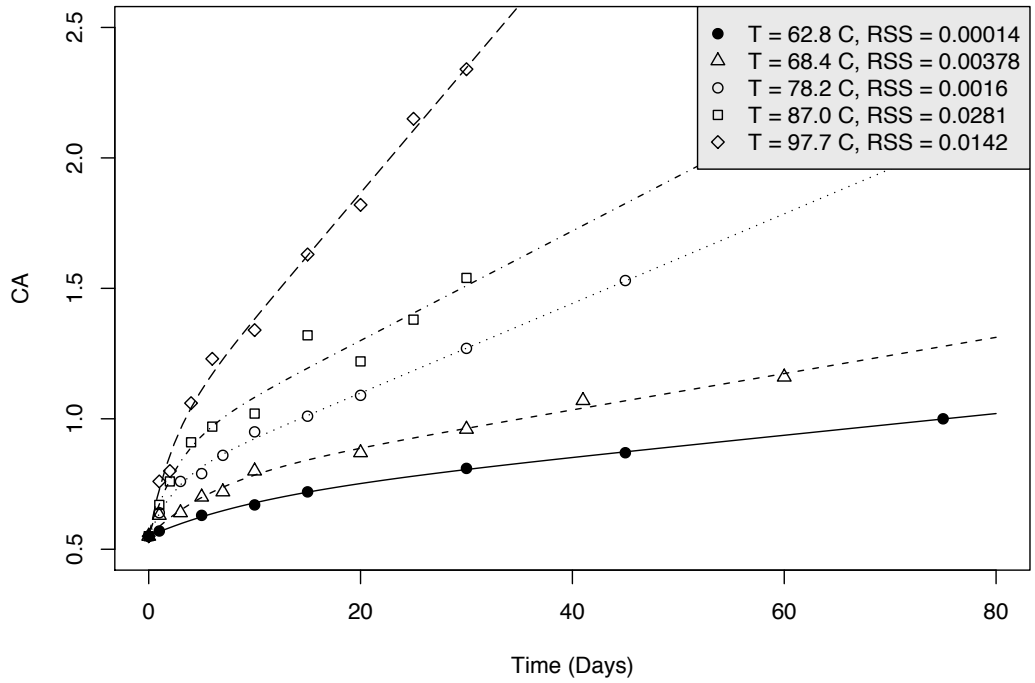

FIGURE 2-25 Nonlinear least square fit of carbonyl area data of SEM 64-22.

TABLE 2-4 M and Reaction Constants of SEM 64-22 (Nonlinear Least Square Fit)

Temperature (°C)	M	k_f	k_c	RSS
62.8	0.1386	0.0977	0.00414	0.00014
68.4	0.2065	0.1600	0.00695	0.00378
78.2	0.2056	0.4111	0.0172	0.001596
87.0	0.3301	0.3739	0.0210	0.02813
97.7	0.3561	0.4619	0.04798	0.01423

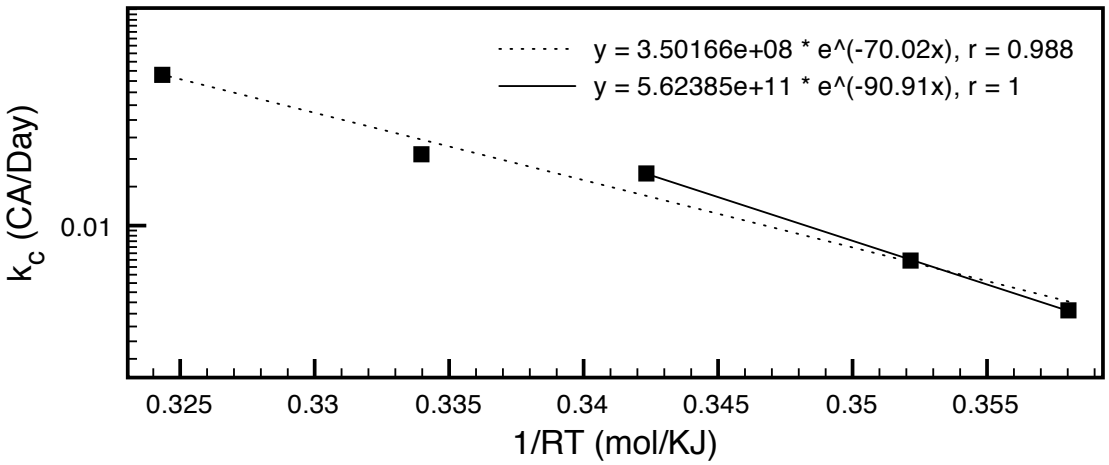

FIGURE 2-26 E_a and A for constant-rate reaction (SEM 64-22).

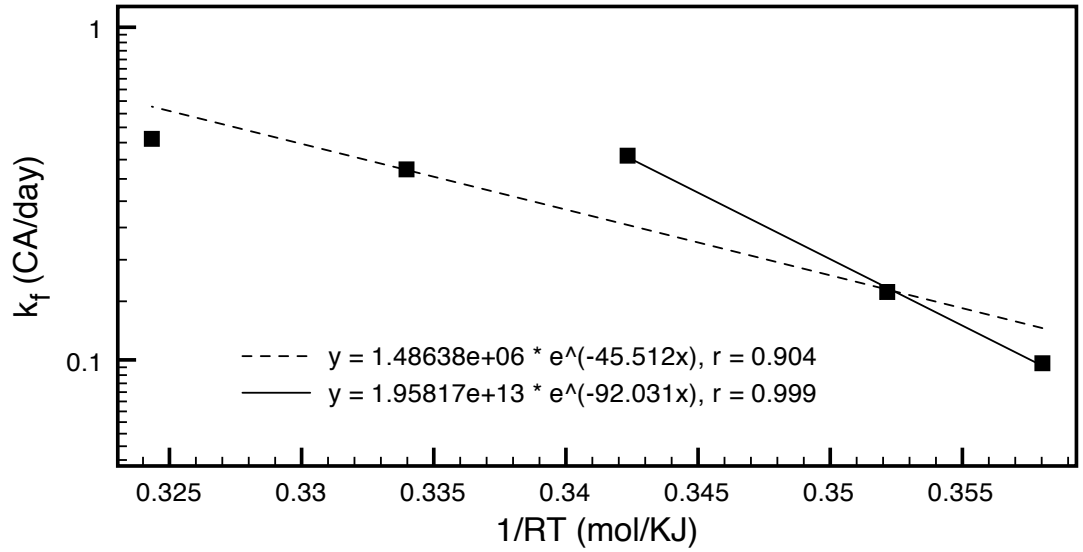

FIGURE 2-27 E_a and A for hypothetical first order reaction (SEM 64-22).

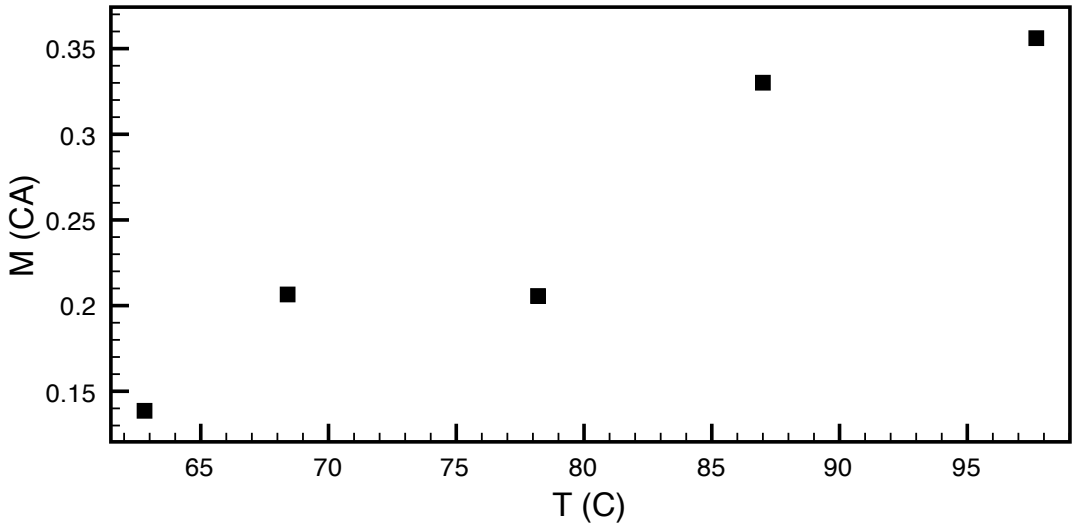

FIGURE 2-28 M value for hypothetical first order reaction (SEM 64-22).

The same analysis approach is applied for CA data of SEM 70-22. Results are shown in Figure 2-29 through 2-32, and tabulated in Table 2-5. Data of 78.2 and 87.0 °C are not obtained due to singularity problem during nonlinear least square estimation, which means the proposed model cannot fit the data at these two temperatures.

TABLE 2-5 M and Reaction Constants of SEM 70-22 (Nonlinear Least Square Fit)

Temperature (°C)	M	k_f	k_c	RSS
62.8	0.3687	0.0492	0.00036	0.005378
68.4	0.1671	0.3470	0.00761	0.03217
97.7	0.2891	0.6580	0.04725	0.004283

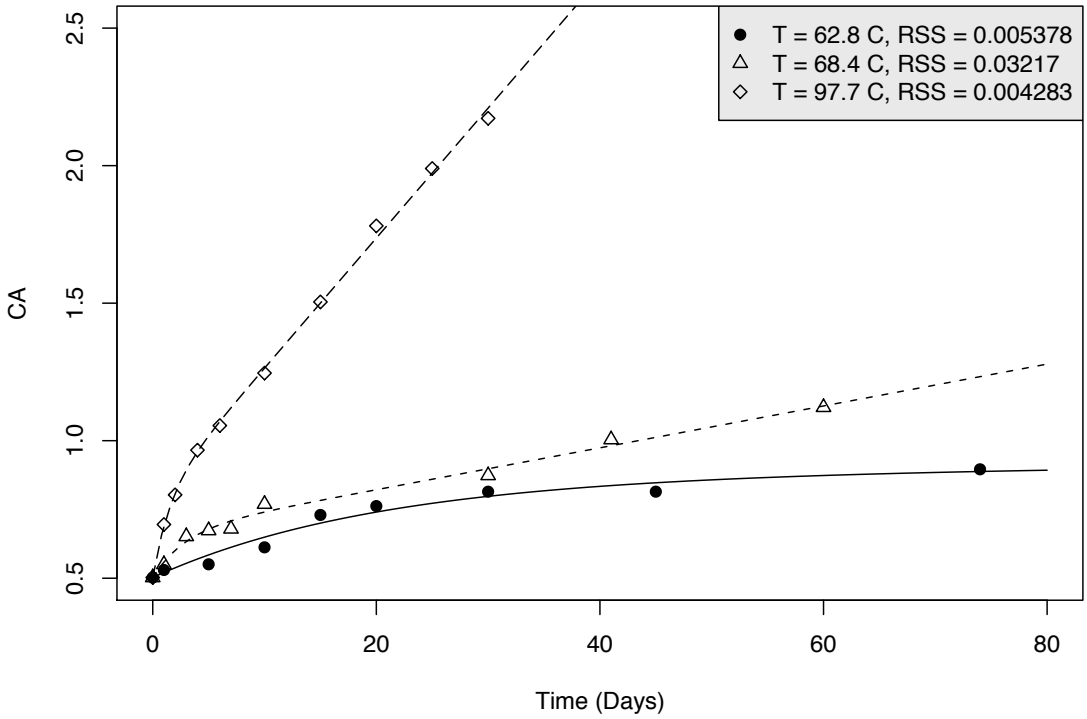

FIGURE 2-29 Nonlinear least square fit of carbonyl area data of SEM 70-22.

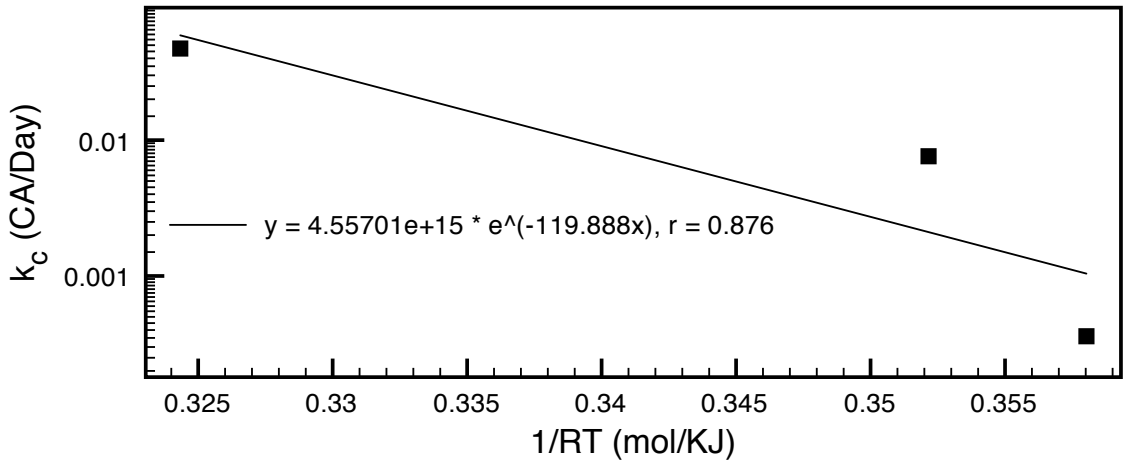

FIGURE 2-30 E_a and A for constant-rate reaction (SEM 70-22).

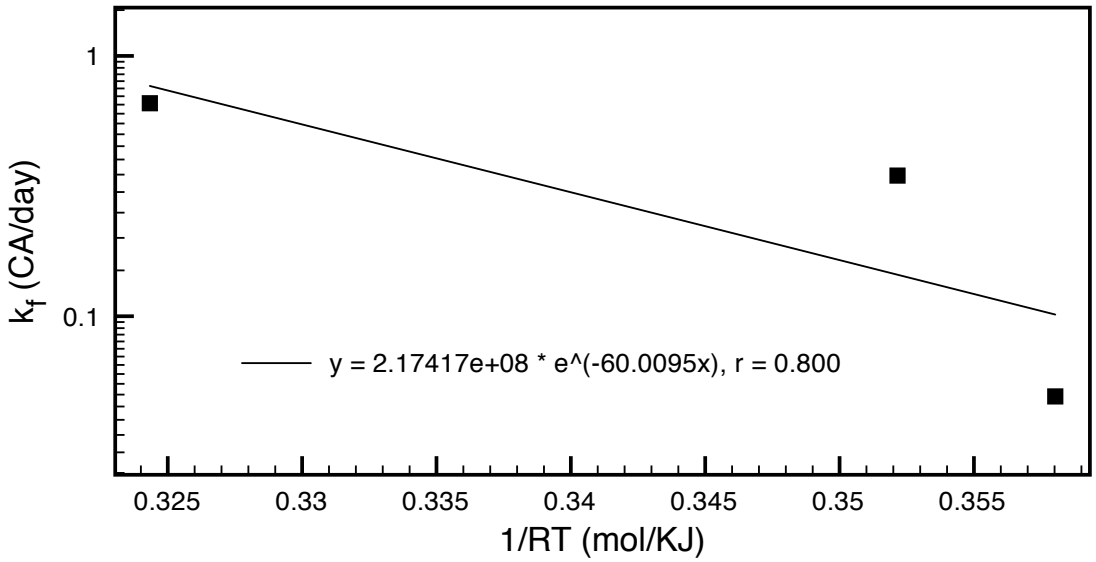

FIGURE 2-31 E_a and A for hypothetical first order reaction (SEM 70-22).

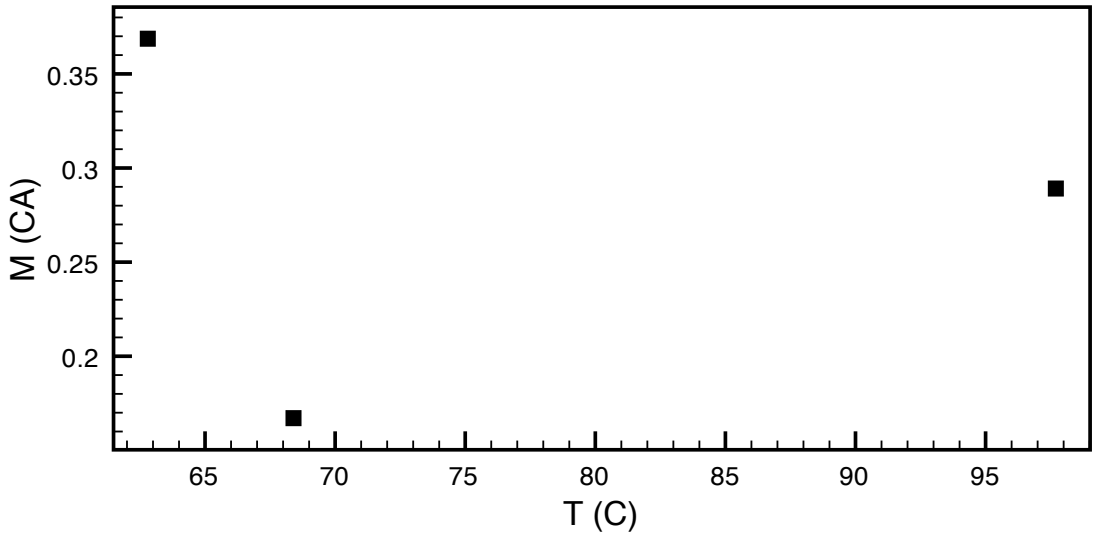

FIGURE 2-32 M value for hypothetical first order reaction (SEM 70-22).

Summary

In this chapter, literature on asphalt oxidation during the early fast-rate period was reviewed. Study of oxygen absorption by tar oil and viscosity change of oxidized binder all suggest that carbonyl area formation should follow a two parallel reaction model, a first order reaction and a zero order constant-rate reaction.

Carbonyl area data of one unmodified binder (SEM 64-22) and one modified binder (SEM 70-22) aged in POVs at five temperatures were obtained. Data show partial agreement with the proposed parallel reaction model. These data are analyzed for binder oxidation kinetics using two methods. One method analyzes data for the constant-rate reaction kinetics first then the first-order reaction kinetics. The other method fits data to the two-reactions model globally for each temperature. These two methods show comparable results for SEM 64-22, especially for data at three lower temperatures. The proposed model fits low temperature CA data of SEM 64-22 extremely well. Similar results are not obtained for data of polymer-modified SEM 70-22. This suggests the parallel model might not be suitable for polymer-modified binder. However, more data are needed to verify.

In summary, no clear conclusion can be drawn at this point. More research is required to fully understand oxidation kinetics of asphalt binder during the early fast-rate period.

CHAPTER III

MODELING HOURLY AIR TEMPERATURE BASED ON PATTERN FROM TIME SERIES ANALYSIS

Prediction of binder oxidation in pavement requires input of accurate hourly pavement temperature. Hourly pavement temperature can be calculated from hourly air temperature and other inputs using a heat transfer model (*12, 13*). In this chapter, a novel method is developed to model hourly air temperature to facilitate the application of pavement temperature model. The new model estimates hourly air temperature from a statistical daily pattern, daily average, maximum and minimum temperature. The pattern is obtained from time series analysis of an entire year of hourly measured data. It represents the most common profile of daily temperature. The new model is compared with the conventional sinusoidal model. Statistical analysis of the result demonstrates that the new model yields better overall results. Further application of the new model is also discussed.

Background

As mentioned previously in Chapter I, the rate of binder oxidation is highly temperature dependent. To predict binder oxidation in pavement, hourly pavement temperature data at different depths are required. While measured data can be obtained from the Long Term Pavement Performance (LTPP) database, these data are usually limited in time span of measurement. In addition, missing data scatter randomly throughout the data set. A more practical method for obtaining temperature profiles is to use model prediction.

Previous work by Hermansson (*12, 13*) developed a thermal transport model that assumes a surface heat flux boundary condition and solves the heat conduction equation in pavements using a numerical method to calculate hourly pavement temperature. Figure 3-1 shows a schematic of heat transfer at the pavement surface and heat conduction in pavement. The prediction results show good agreement with measurements obtained from the LTPP database. For the pavement sites studied, a maximum monthly average absolute error of 2.0 °C is reported (*13*).

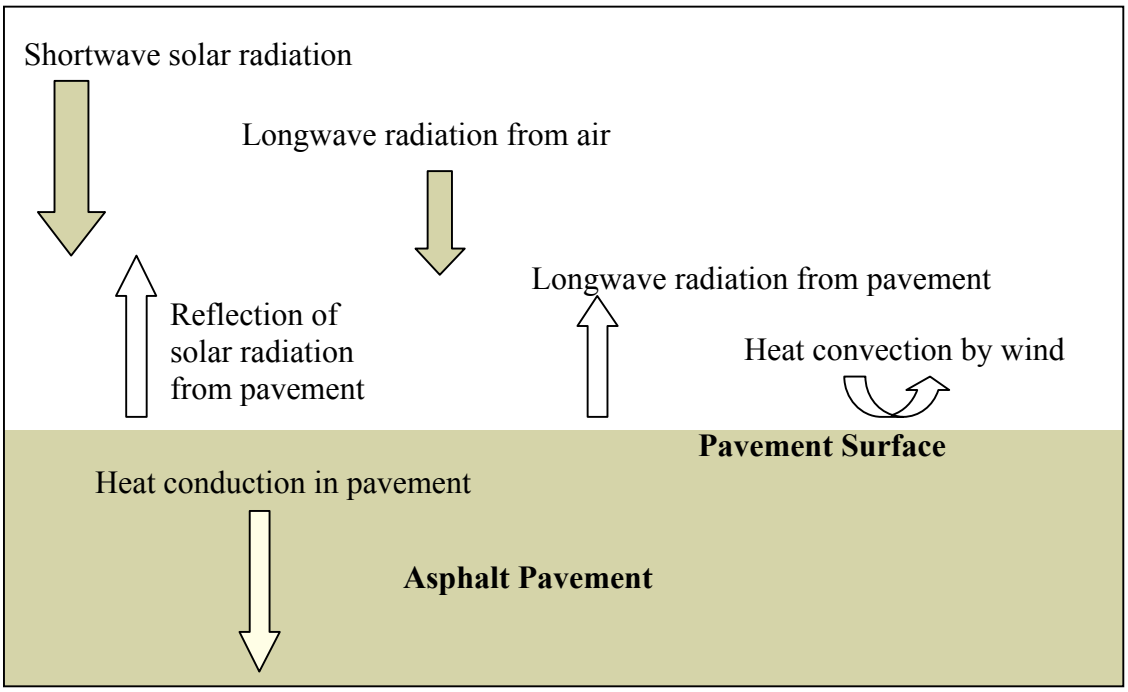

FIGURE 3-1 Schematic heat transfer model of pavement.

The thermal transport model requires hourly ambient air temperature among other inputs, such as hourly solar radiation and wind speed. As shown in Figure 3-1, air exchanges heat with pavement through heat radiation and convection.

Some measured hourly air temperature data can be found in the National Climate Data Center (NCDC) and the LTPP database. However, measured data are limited in time range and mixed with missing data. Fortunately, most weather stations record only maximum, minimum, and average air temperature, and missing data are very rare. Therefore, an efficient way to obtain hourly air temperature data is modeling them from maximum, minimum, and average temperature.

Conventional Air Temperature Model

The conventional air temperature model assumes that air temperature variation is a sinusoidal function of time around the average temperature (*24*). It can be expressed in the following equations:

$$T(t) = \frac{T_{\max} - T_{\min}}{2} \cdot \cos\left[\frac{2\pi(t-15)}{24}\right] + T_{av} \tag{3-1}$$

$$T_{av} = 0.525T_{\max} + 0.464T_{\min} - 0.229 \tag{3-2}$$

where T_{max} and T_{min} are maximum and minimum air temperature, T_{av} is average temperature, which can be calculated from maximum and minimum.

Equation 3-1 implies that the maximum air temperature occurs at 3 PM and minimum occurs at 3 AM, everyday. The constants in Equation 3-2 are obtained from linear regression of measured data.

Figure 3-2 shows a model calculation of 24-hour air temperature using Equations 3-1 and 3-2 with 24-hour measured data of a typical day. From the comparison, it is obvious that 1) the time between maximum and minimum temperature may not equal to 12 hours and 2) the temperature profile of 24 hours does not match

sinusoidal function. These two intrinsic disadvantages of the conventional sinusoidal model lead to estimation errors that cannot be alleviated by parameter optimization.

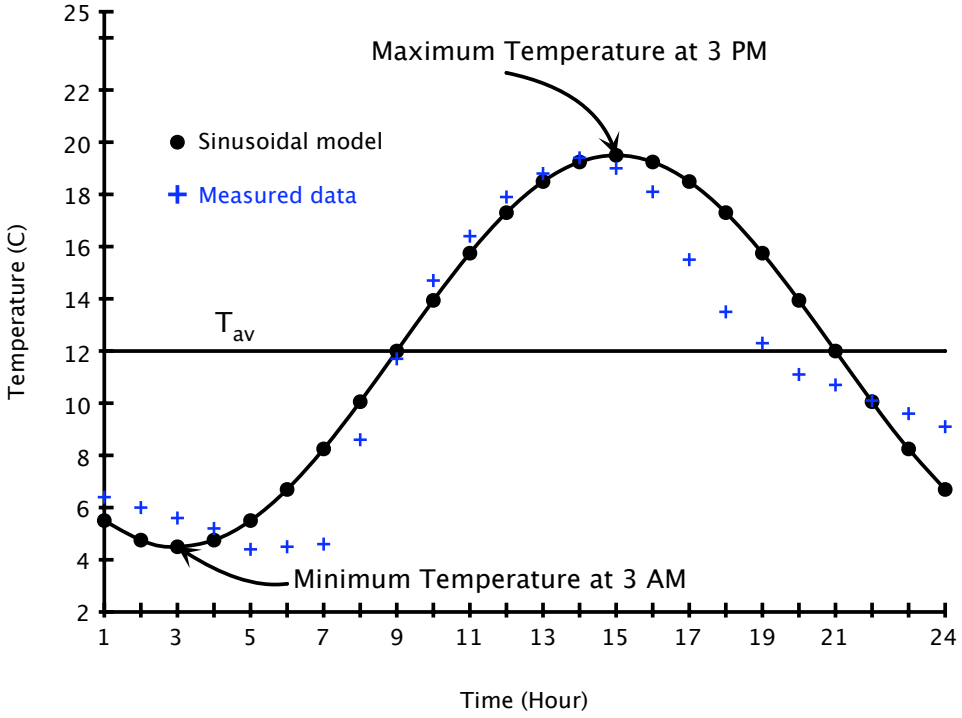

FIGURE 3-2 Comparison of sinusoidal model calculation with measured air temperature profile.

New Air Temperature Pattern Model Using Time Series Analysis

Rough observations of measured air temperature at different scales show that while hourly air temperature profiles of certain days show arbitrary behavior, most of them follow a pattern. This pattern represents the fluctuation of hourly air temperature around daily average temperature more realistically. By using such a pattern instead of a sinusoidal function in conventional model, a better air temperature model is herein developed.

The following steps show the methodology of the new air temperature pattern model:

1. Daily average, maximum and minimum data, from which hourly air temperature will be modeled, are collected from the NCDC database for the location of interest.
2. An entire year of measured hourly air temperature data are collected from the LTPP database for that location. If data for the exact location are not available, data for nearby location can be used. This part is further discussed in a later section.
3. Seasonal-trend decomposition of time series analysis (*25*) shown in Equation 3-3 is applied to the hourly air temperature data. A pattern, specific to the location where measurements are taken, is obtained.

$$T = trend + pattern + \varepsilon \tag{3-3}$$

   where T is measured data, *trend* is the change of daily average temperature over an entire year, *pattern* is a periodic function repeating each day, and ε is the remainder after *trend* and *pattern* are extracted from measured data.
4. Linear approximation of daily average data disaggregates them into hourly resolution, for each two successive days. This step gives the trend of daily average temperature over an entire year.
5. The pattern is added to disaggregated daily average temperature of each day for the entire year.

6. Finally, the result is linear-transformed locally to match the maximum and minimum data, according to Equation 3-4.

The linear transformation of the sum of the pattern and disaggregated daily average data is expressed in the following equation:

$$\hat{T}(i) = \hat{T}_{\min} + [T(i) - T_{\min}] \cdot \frac{\hat{T}_{\max} - \hat{T}_{\min}}{T_{\max} - T_{\min}} \quad (3\text{-}4)$$

where $T(i)$ and $\hat{T}(i)$ are the temperature before and after linear transformation, i is time (in hour), $\hat{T}_{\max}$ and $\hat{T}_{\min}$ are the measured maximum and minimum temperature, T_{max} and T_{min} are the maximum and minimum before linear transformation. Equation 3-4 is applied locally for temperature between two adjacent maximum and minimum temperatures.

Case Study

To demonstrate the methodology of the new pattern model, a pavement site located in Brazos County, Texas, is selected. Measured daily average, maximum and minimum air temperature data of an entire year are taken from the Automatic Weather Station (AWS) module of the LTPP database. The AWS ID for this site is 48-0801.

Measured hourly air temperature data are also obtained from the same source. These data are decomposed into the three components in Equation 3-3, as shown in Figure 3-3. Figure 3-3 contains fours rows. The first row shows the measured hourly air temperature. The second row is the repetitive pattern component, which is the part of the new model. It is obtained by applying local polynomial regression fitting to data after trend component is subtracted from raw data. This part clusters due to the big time

range. Figure 3-4 shows this part clearly over five days. The third row is the trend component. It is estimated from moving average of 24-hour window. It represents daily average temperature and follows the measured data exactly through the year. The fourth row is the remainder ε. It embodies the random effect of rain, cloud, and other weather conditions on air temperature.

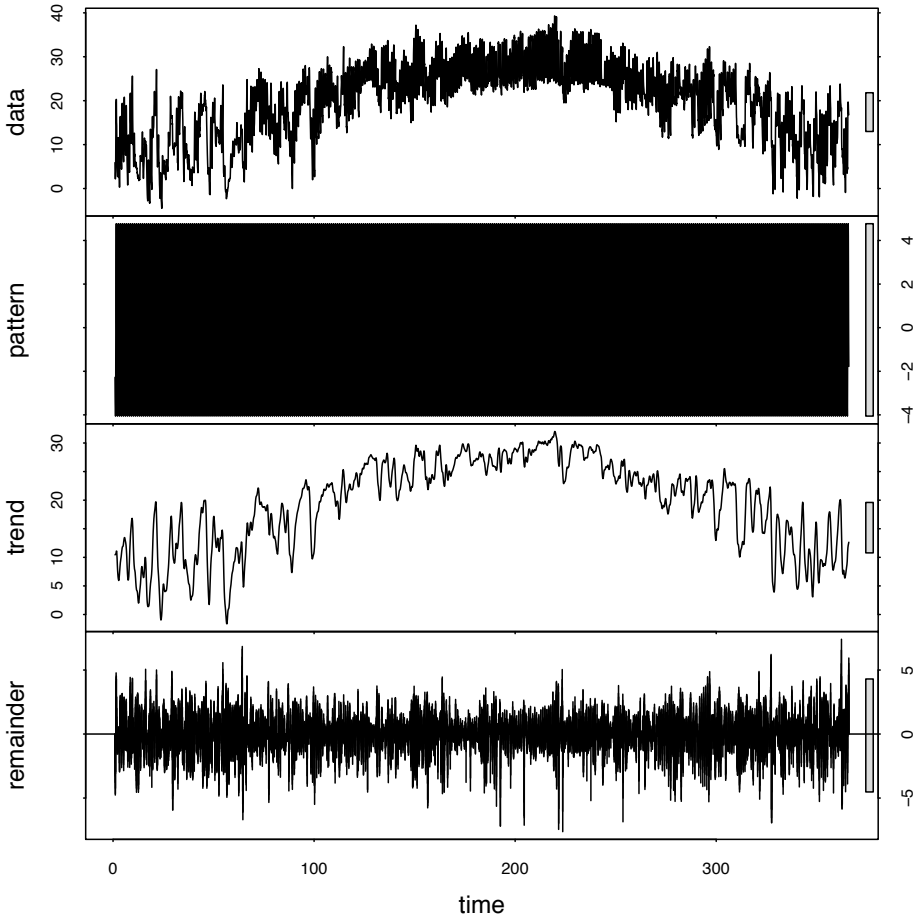

FIGURE 3-3 Seasonal-trend decomposition of hourly air temperature for an entire year.

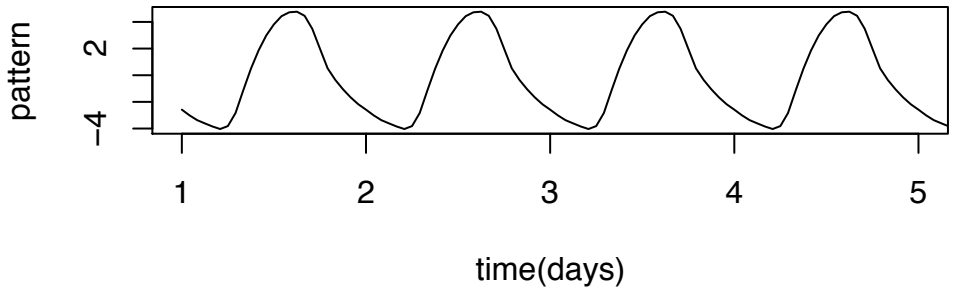

FIGURE 3-4 Pattern component shown for 5 days.

Among the three parts in Figure 3-3, the greatest interest is pattern component. Figure 3-4 shows a clear view of this part over 5 days. Comparing this pattern to the 24-hour air temperature profile in Figure 3-2, two important similarities are observed. First, they are both a non-sinusoidal shape. This indicates that air temperature increases quicker after sunrise and decreases slower during the night. Second, the times of maximum and minimum temperature are not necessarily 3 AM and 3 PM, and the time between them is usually less than 12 hours. Because the pattern is obtained from analysis of an entire year of measured data, it is more robust and representative of the hourly air temperature fluctuation.

Next, daily average air temperature in hourly resolution is estimated using linear approximation of daily average data. The periodic pattern (also in hourly resolution) from a previous time series analysis is then added to that for each day over an entire year.

Finally, the result is linearly transformed using Equation 3-4 to fit daily maximum and minimum data. This step accounts for the remainder ε in a sense that the maximum and minimum temperatures are representative of extreme weather conditions.

Figure 3-5 illustrates temperature profile before and after linear transformation, along with measured data. From Figure 3-3, the advantage of linear transformation is clearly observed, in preserving the shape of temperature profile.

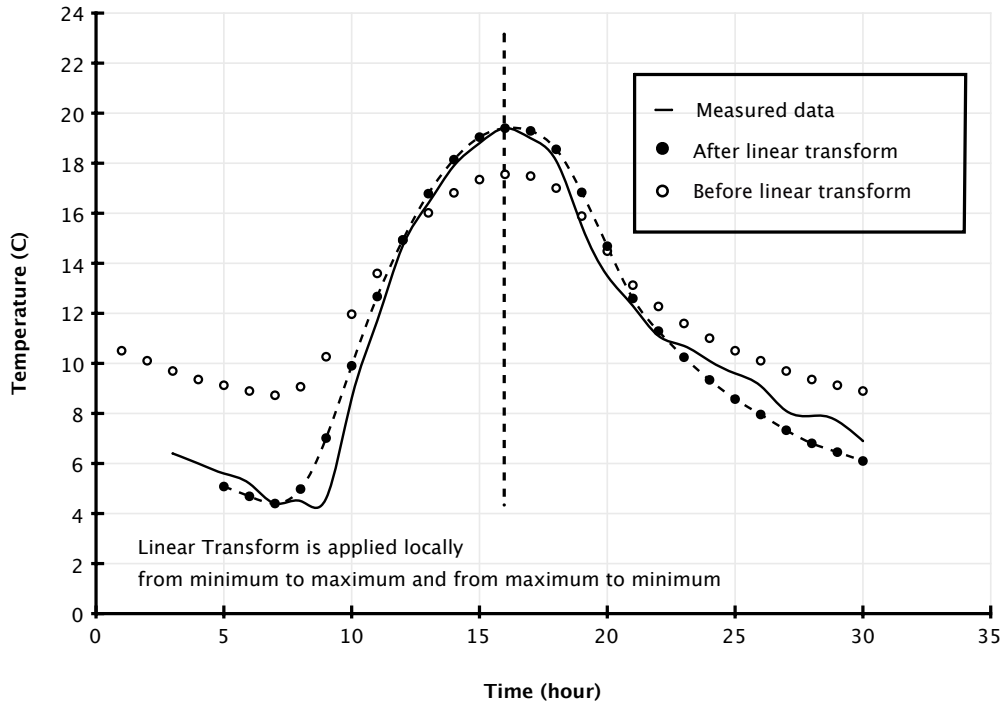

FIGURE 3-5 Comparison of air temperature calculations before and after linear transformation with measured data.

Comparison of Pattern Model and Sinusoidal Model

Hourly temperature data are estimated from daily average, maximum and minimum temperature data, using the new pattern model and sinusoidal model, respectively. Model estimations are compared with measured data. Mean square errors (MSE) are calculated to evaluate accuracy of model estimation.

$$MSE = \frac{\sum_1^N (\hat{T}_i - T_i)^2}{N} \tag{3-4}$$

where N is the total number of hours, $\hat{T}_i$ is estimated temperature, and T_i is measured temperature.

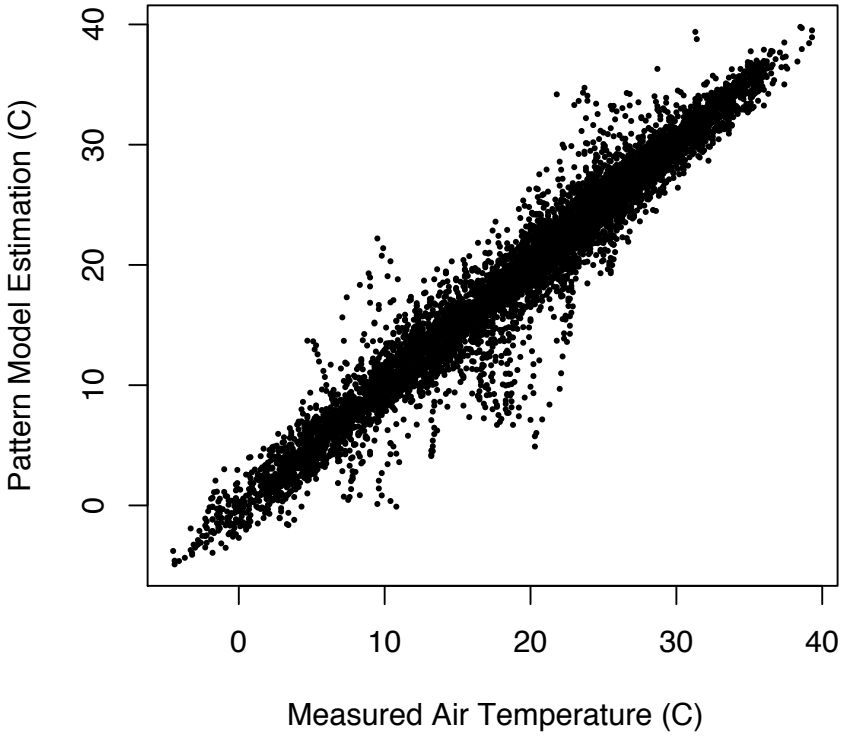

FIGURE 3-6 Comparison of pattern model estimated hourly air temperature with measured temperature over a year.

Figure 3-6 shows the comparison of pattern model estimation of hourly air temperature with measured data for year 2003 from AWS site 48-0801. Figure 3-7 shows the comparison of sinusoidal model estimation with the same measured data.

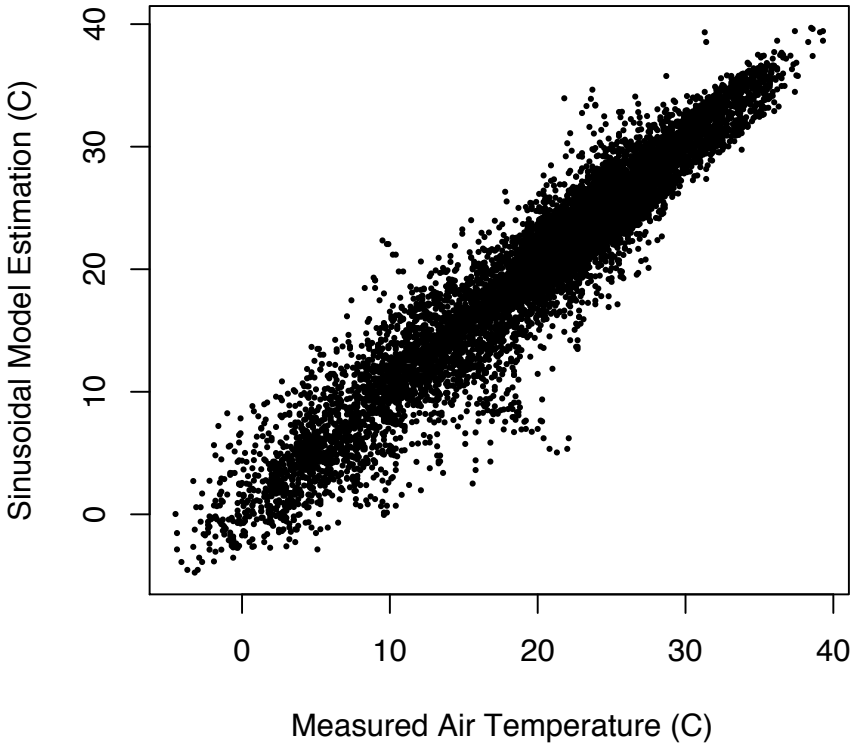

FIGURE 3-7 Comparison of sinusoidal model estimated hourly air temperature with measured temperature over a year.

By comparing Figure 3-6 and 3-7, it is clear that pattern model of this work is significantly better than sinusoidal model. The results obtained from the pattern model are more aggregated to y=x line, especially at low and intermediate temperatures. This is probably due to good match of the pattern with the measured temperature profile during midnight and before sunrise. In addition, MSE values are 3.833 for the pattern model and 6.817 for the sinusoidal model.

Model comparisons are also conducted for states located in different climate regions across the United States. Measured hourly and daily air temperature data of an entire year are collected from the AWS module of the LTPP database. Table 3-1 lists the states

studied, corresponding AWS ID, year of temperature, and MSE values for model estimation. It is clear that the pattern model consistently yields better estimation results than the sinusoidal model, especially for sites in California and Kansas.

TABLE 3-1 Comparison of Model Estimation for 9 States in U.S.

Location	AWS ID	Year	MSE of Pattern Model	MSE of Sinusoidal Model
Arizona	040100	2004	3.060	3.679
California	060200	2002	2.292	6.024
Kansas	200100	2002	5.783	11.155
Montana	300800	2002	6.499	10.529
Nevada	320200	2002	5.193	9.084
New York	360800	2003	6.740	8.457
South Dakota	460800	2004	7.904	12.974
Brazos, Texas	480801	2003	3.833	6.817
Hidalgo, Texas	480113	2004	2.336	4.592
Bell, Texas	48A807	2003	5.062	7.044
Utah	490800	2003	7.000	9.110

Application of the Pattern Model

An interesting question that dramatically affects the application of the pattern model is: can the same pattern obtained from one pavement site be applied to another one? If yes, what are the limitations?

To answer these questions, temperature patterns for Texas, Nevada, and New York are plotted together in Figure 3-8. The three patterns of three counties in Texas are quite close to each other, suggesting one pattern might be used for locations in the same state or same climate region. The difference between New York pattern and others is obvious. Thus for locations far apart, the use of offsite patterns is not recommended.

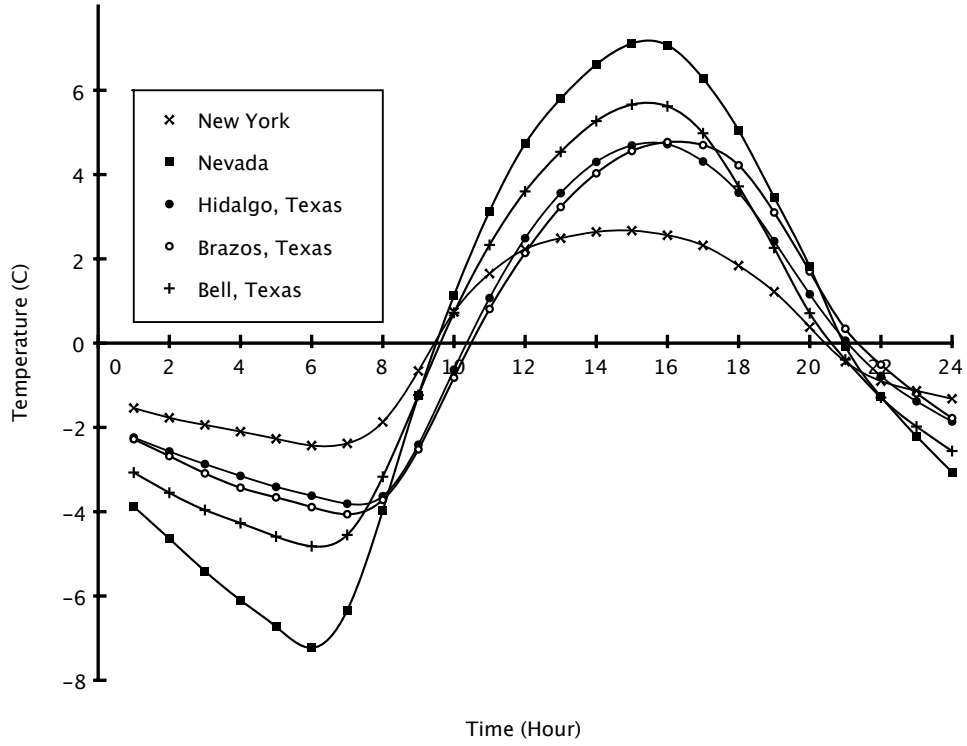

FIGURE 3-8 Temperature patterns of six locations.

To further demonstrate the applicability of offsite patterns, the pattern of Bell, Texas (AWS ID 48A807), is used in estimation of air temperature for Brazos and Hidalgo, Texas, yielding MSEs of 4.401 and 2.800, respectively. Comparing with MSEs

in Table 3-1, these offsite pattern estimates are not as good as onsite ones, but are still better than the sinusoidal model.

Summary

In this chapter, a novel pattern model is developed to more accurately estimate hourly air temperature from daily average, maximum and minimum temperatures. The new model utilizes a non-sinusoidal pattern of air temperature fluctuation around the average temperature. The pattern is obtained from time series analysis over an entire year of measured hourly data, and thus follows air temperature change closer than sinusoidal function.

Pattern model estimations are compared with sinusoidal modeling for 11 locations in 9 states across the U.S. MSE evaluations demonstrates that the new model always yields better results than the conventional sinusoidal model.

Application of an offsite pattern is also examined. Although the offsite pattern model can still predict reasonable results, use of an onsite pattern is recommended when available.

CHAPTER IV

GRAPHIC USER INTERFACE FOR PAVEMENT AGING AND FATIGUE ANALYSIS

In this chapter, a detailed description of the graphic user interface for pavement aging and fatigue analysis, namely Pavement Aging and Fatigue Analyzer (PAFA), is presented, followed by a case study to illustrate its application. The software incorporates research findings on binder oxidation kinetics, the oxygen transport model in pavement, and the CMSE fatigue analysis system reviewed in Chapter I. Chapter II provides a preliminary model for the fast-rate period of binder aging, and the new pattern-based air temperature model developed in Chapter III calculates hourly air temperature as input for pavement temperature calculation. The pavement temperature model is not implemented as part of the software. Hence, hourly pavement temperature should be provided as an input data file.

Introduction

PAFA is based on extensive studies of binder aging in the laboratory (*3, 4, 7, 8, 9*) and a recently developed CMSE mixture fatigue analysis method (*5, 17, 18*). Mixture fatigue life is defined as the number of loading cycles a mixture can bear under repeated loading before severe performance deterioration. It is characterized by several mixture laboratory tests, outlined in TxDOT project 0-4468 (*17*), including Tensile Strength (TS) test, Direct Tension (DT) test, Repeated Direct Tension (RDT) test, and surface energy (SE) measurement of binder and aggregate. It is also found that mixture fatigue life

declines significantly with binder aging. As binder ages, carbonyl area increases, as well as viscosity and DSR function.

PAFA mainly consists of two parts: 1) prediction of binder oxidation using oxygen transport model and hourly pavement temperature (measured or calculated) and 2) calculation of mixture fatigue life using the CMSE approach. These two parts address the two issues associated with MEPDG discussed in Chapter I, the GAM model and fatigue cracking model (Equation 1-1), respectively. Figure 4-1 shows the procedures implemented beneath the graphic interface.

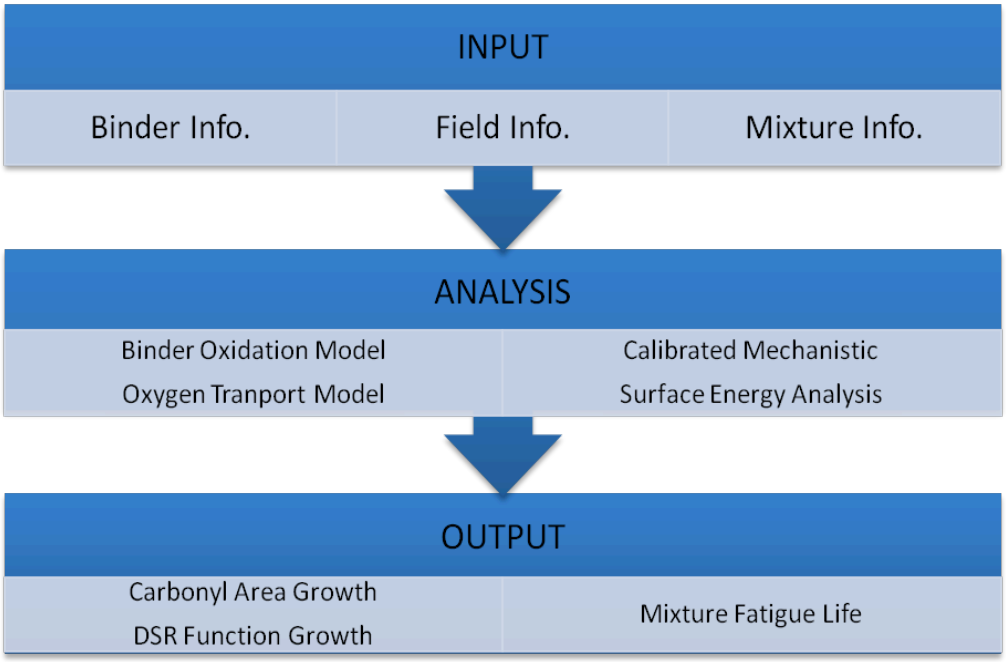

FIGURE 4-1 Procedures implemented in PAFA graphic user interface.

The analysis process includes the following steps:

1. The partial differential equation of oxygen diffusion and reaction is solved for oxygen partial pressure as a function of time, temperature, and position in binder film;
2. Carbonyl area is calculated using binder aging model with input of pavement temperature data and oxygen partial pressure data calculated from step 1;
3. DSR function growth with time is calculated from carbonyl area and DSR function hardening susceptibility (HS);
4. Mixture fatigue life at unaged state is calculated based on CMSE approach with input from various mixture tests;
5. Mixture fatigue life decline is obtained from the correlation of DSR function and fatigue life with input from steps 3 and 4.

The PAFA software provides:

1. An interface to input various information,
2. computational engines for aging prediction and fatigue performance, and
3. plot of results and numeric outputs from the analyses in spreadsheets.

It is important to note that other important factors, which affect pavement fatigue performance, are not considered in PAFA. For example, moisture damage will decrease adhesive and cohesive bond strength, leading to pavement that is more susceptible to cracking. Therefore, PAFA still needs further improvement and should be used as a preliminary tool for evaluation of pavement aging level and fatigue resistance.

Installation

The software is developed for a Windows® Operating System. The program is written in MathWorks' MATLAB®, and compiled using MATLAB Compiler into binaries. If MATLAB is already installed on the computer, the program can be run directly. Otherwise, the MATLAB Component Runtime (MCR) Library must be installed as a pre-requirement in order to use the program in Windows without installation of MATLAB. The MCR Library can be downloaded from website of MathWorks Partner (http://www.sferic.com/Matlab/CompilerRunTime.htm).

Using PAFA

After the software is installed, the PAFA graphic user interface (GUI) can be invoked by double click PAFA.exe. A GUI will appear as shown in Figure 4-2.

The interface is divided into four parts: 1) Binder Information, 2) Mixture Information, 3) Field Information, and 4) "Run Analyzer" Button. After the user enters required information, by clicking the "Run Analyzer" button, carbonyl area, DSR function, and pavement fatigue life will be calculated and plotted as a function of time. The following sections will explain the input information in detail.

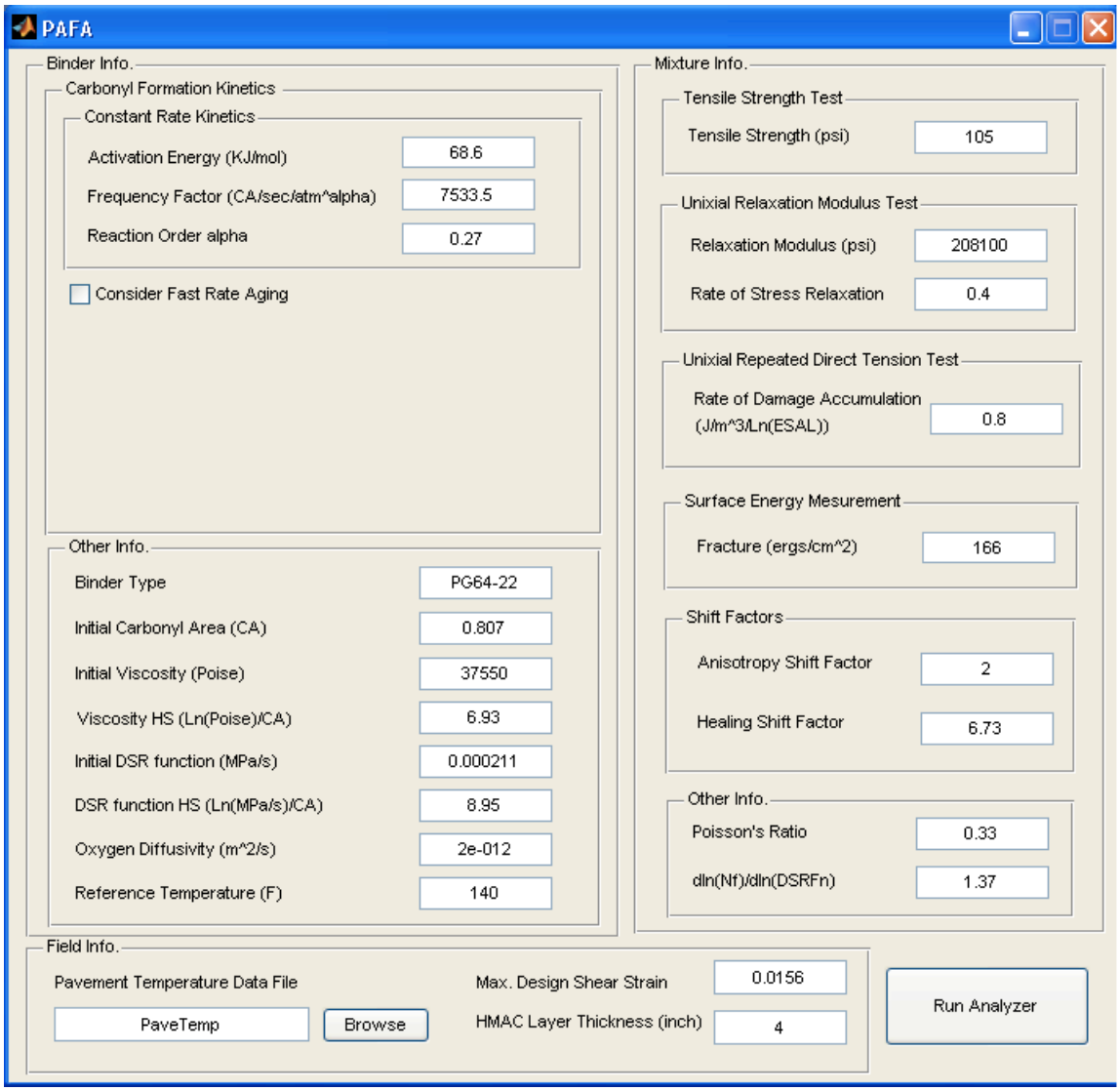

FIGURE 4-2 PAFA graphic user interface.

Input Binder Information

Binder information is needed to calculate binder oxidation in pavement. It is categorized into two parts: Carbonyl Formation Kinetics and Other Information.

As binder ages in pavement, carbonyl group products are formed. Carbonyl area growth experiences two different stages, an early fast-rate period followed by a

constant-rate period. In hot climate region, such as Texas, fast-rate kinetics are usually passed during the first year of pavement construction; therefore, the fast-rate period is of secondary importance with respect to long-term pavement performance such as fatigue cracking resistance. However, in cold states, such as Minnesota, the fast-rate period could last over ten years due to cold pavement temperature and consequently slow aging rate. Detailed argument can be found in Chapter II of this work.

Depending on the climate region (hot or cold) in which pavement is located, a user might wish to consider binder aging in the early fast-rate period. Therefore, in this part, the user has the freedom to choose whether or not to consider fast-rate aging, by checking or unchecking the checkbox “Consider Fast Rate Aging”.

Due to a lack of sufficient experimental data to verify the kinetics of fast-rate aging, it is not implemented yet. However, the software interface is designed with fast-rate in mind. As soon as fast-rate kinetics are clear, they can be incorporated into the software.

In contrast to fast-rate aging, constant-rate aging is well understood and should always be considered because it is the most important cause of binder hardening and consequent deterioration of mixture performance. Based on the proposed aging model in Chapter I, activation energy, frequency factor, and reaction order with respect to oxygen partial pressure are required. The units of these parameters are listed in Table 4-1.

TABLE 4-1 Constant-rate Kinetics of Carbonyl Formation

Parameter	Unit
Activation Energy	KJ/mol
Frequency Factor	$CA/(s \cdot atm^{\alpha})$
Reaction Order (α) with respect to Oxygen Pressure	dimensionless

The "Other Info." part lists other important information, including binder type, initial carbonyl area, initial low shear rate limiting viscosity, viscosity HS, initial DSR function, DSR function HS, oxygen diffusivity in virgin asphalt, and the reference temperature at which the initial viscosity is measured. Their units are listed in Table 4-2.

TABLE 4-2 Other Important Binder Information

Parameter	Unit
Initial Carbonyl Area	CA
Initial Viscosity	Poise
Initial Viscosity HS	Ln[Poise]/CA
Initial DSR Function	MPa/s
DSR Function HS	Ln[MPa/s]/CA
Oxygen Diffusivity	m^2/s
Reference Temperature	F

Input Mixture Information

The majority of mixture information can be obtained from experiments specified for the CMSE approach in TxDOT project 0-4468 (*17*). Mixture information is grouped according to mixture tests, i.e. TS test, uniaxial RM test, uniaxial RDT test and SE measurement. Shifting factors which shifts laboratory test results to match complex field conditions are also considered. The anisotropy shift factor (typical value is 2.0) accounts

for anisotropic loading due to directional traffic. The healing shift factor accounts for healing/closure of fracture surface in mixture.

Other information includes Poisson's ratio and the rate of decline of fatigue life with DSR function increase, in log-log scale. This parameter characterizes the negative effect of binder oxidation and hardening on mixture fatigue. Units of mixture input parameters are shown in Table 4-3.

TABLE 4-3 Mixture Input from Mixture Tests

Parameter	**Unit**
Tensile Strength	Psi
Relaxation Modulus	Psi
Rate of Stress Relaxation	Dimensionless
Rate of Damage Accumulation	(J/m^3)/Ln(EASL)
Fracture Energy	$Ergs/cm^2$
Anisotropy Shift Factor	Dimensionless
Healing Shift Factor	Dimensionless
Poisson's ratio	Dimensionless
dLn(Nf)/dLn(DSRFn)	Ln[EASL]/Ln[MPa/s]

Input Field Information

Field information includes the pavement temperature profile, hot mix asphalt concrete (HMAC) layer thickness, and maximum design shear strain, which is computed at the edge of a loaded tire. Field information, especially pavement temperature, is important because it affects the rate of binder aging and mixture performance.

In the PAFA interface, hourly pavement temperature data can be selected by: 1) filling in the file name if the data file is at the same directory of the program or 2) browsing through the file system.

One important feature is that the time range of the hourly pavement temperature determines the time range of software calculation. For example, if temperature data file contains one month of data, the software will calculate carbonyl area growth, etc. for that one month.

Hourly pavement temperature data are required to accurately calculate binder aging rate and carbonyl area growth. They can be downloaded from Long Term Pavement Performance (LTPP) database for limited pavement sites and limited time ranges. Otherwise data can be calculated using a pavement temperature prediction model and program (*11, 12, 13*). The model is based on first principle heat transfer fundamentals and requires hourly air temperature, hourly solar radiation, and daily wind speed data as inputs.

Format of Hourly Pavement Temperature Data File

To utilize pavement temperature data (in Excel® format) downloaded from the LTPP database, it is required that the temperature input file be in an Excel® spreadsheet format, and follow exactly the following specification in Table 4-4. From the specification, the spreadsheet has only one column, with the leading five rows providing general information and temperature data starting from 6th row.

Run the Analyzer

After all the information mentioned above is entered through the software interface, the program is ready to run. Click the "Run Analyzer" button; after a few minutes or more depending on the time range you are trying to calculate results for, carbonyl area growth, DSR function growth, and fatigue life decline with time are

plotted. Corresponding data files are also generated and stored in the spreadsheet file 'output.xls' in the same directory of the program.

TABLE 4-4 Format of Hourly Pavement Temperature Data

Row	Information
1	Location of Pavement
2	Depth at which data are measured /calculated
3	Temperature Unit: °C
4	Starting Time (yyyy-mm-dd)
5	End Time (yyyy-mm-dd)
6	Numerical temperature data
…	…

Case Study

To illustrate the application of PAFA software, a case study is presented. The inputs are set up as default values in the software. Therefore, users can run the PAFA analyzer directly and visualize the results.

Suppose a mixture designer is interested in predicting mixture fatigue performance of Route 77 located in Refugio, Texas, the thickness of HMA layer is 10 cm, and the design shear strain is 0.0156. A typical value of Poisson's ratio for the HMA layer is 0.33.

For the case study, a mixture (designated as Bryan) is selected from TxDOT project 0-4468 (*17*), such that mixture test results are available. Therefore, data in the following sections are from 0-4468 (*17*) unless stated otherwise. The mixture consists of 4.4 percent binder (by weight of mixture) PG 64-22 and 95.6 percent limestone aggregate. Healing shift factor and anisotropy shift factor are 6.73 and 2.0 respectively.

The ratio of decline of Ln(N_f) with an increase of Ln(DSRFn) is 1.37. Mixture test results for Bryan mixture are shown in Table 4-5. More experimental data for different mixture design can be found in Chapter V.

TABLE 4-5 Mixture Test Results for Bryan Mixture

Mixture Test	**Parameter**	**Value**
TS Test	Tensile strength at break (psi)	105
RM Test	Relaxation modulus (psi)	208,100
	Rate of stress relaxation	0.4
RDT Test	Rate of damage accumulation (J/m^3)/Ln(EASL)	0.8
SE Measurement	Surface energy of fracture ($Ergs/cm^2$)	166

Binder kinetics data can be obtained from literature or experiment. For this case study, experiment data for binder kinetics are not available for PG 64-22. Data for Cosden AC-20 are used, as shown in Table 4-6.

Table 4-6 Binder Kinetics Data for Cosden AC-20*

Activation Energy (KJ/mol)	**Frequency Factor** ($CA/(s \cdot atm^{\alpha})$)	**α**	**Oxygen Diffusivity** (m^2/s)
68.6	19.86	0.27	20e-13

* Data from Lunsford (14).

Other binder data are available for Bryan PG 64-22, as shown in Table 4-7. Note in this case, the initial CA for Bryan PG 64-22 is measured after short-term aging according to AASHTO PP2 at 135 °C for 4 hours (*26*); thus fast-rate aging has already been already passed.

Table 4-7 Other Binder Data for Bryan PG 64-22

Initial CA	**Initial Viscosity** (poise)	**Viscosity HS**	**Initial DSR function** (MPa/s)	**DSR function HS**
0.807	37550	6.93	2.11e-4	8.95

Pavement temperature data are downloaded from LTPP database for Route 77 in Refugio, Texas, starting from 12/1993 to 11/1994. Data format are slightly modified to meet the data format specified above. Then the file is saved as 'PaveTemp.xls' in the same directory as the program.

After running the program, output data are saved in a spreadsheet file named "output.xls", which contains three worksheets named "Carbonyl Area," "DSR Function," and "Fatigue Life". Figures 4-3, 4-4, and 4-5 are the plots of results.

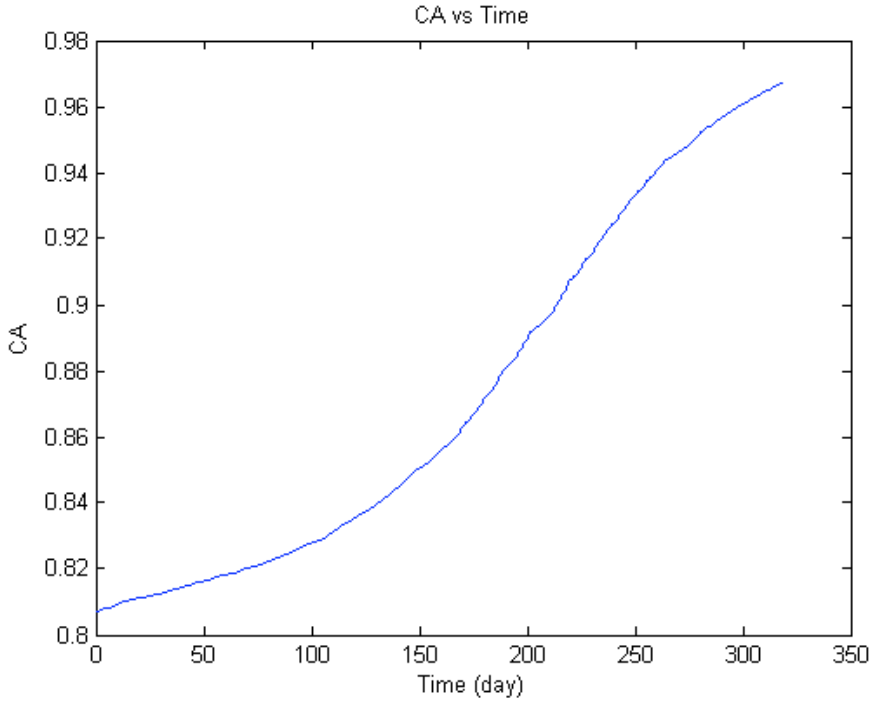

FIGURE 4-3 Carbonyl area increase with time for a whole year.

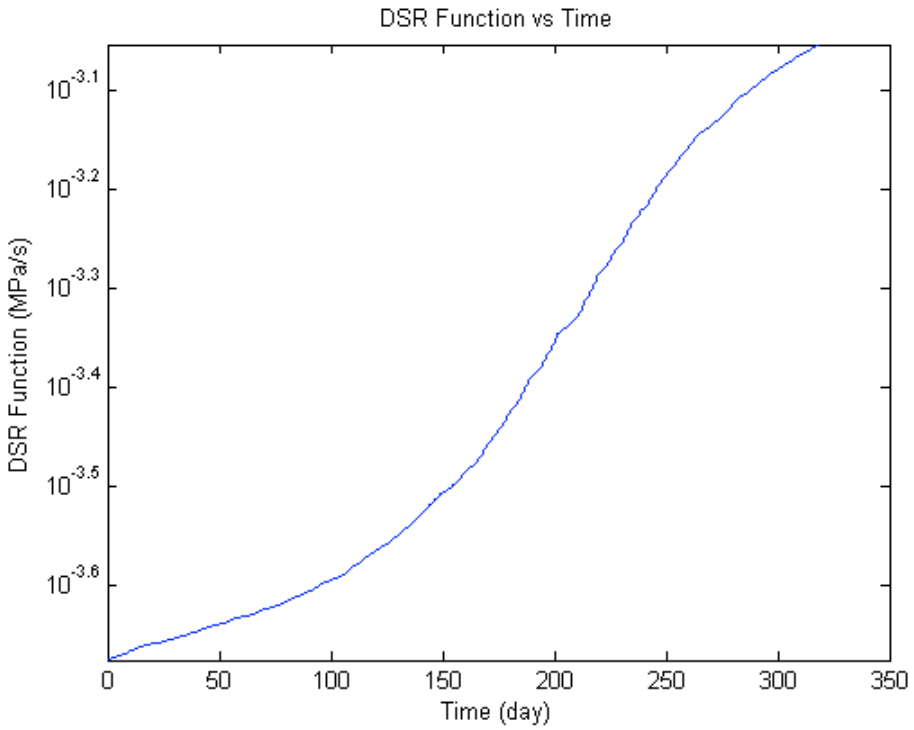

FIGURE 4-4 DSR function increase with time for a whole year.

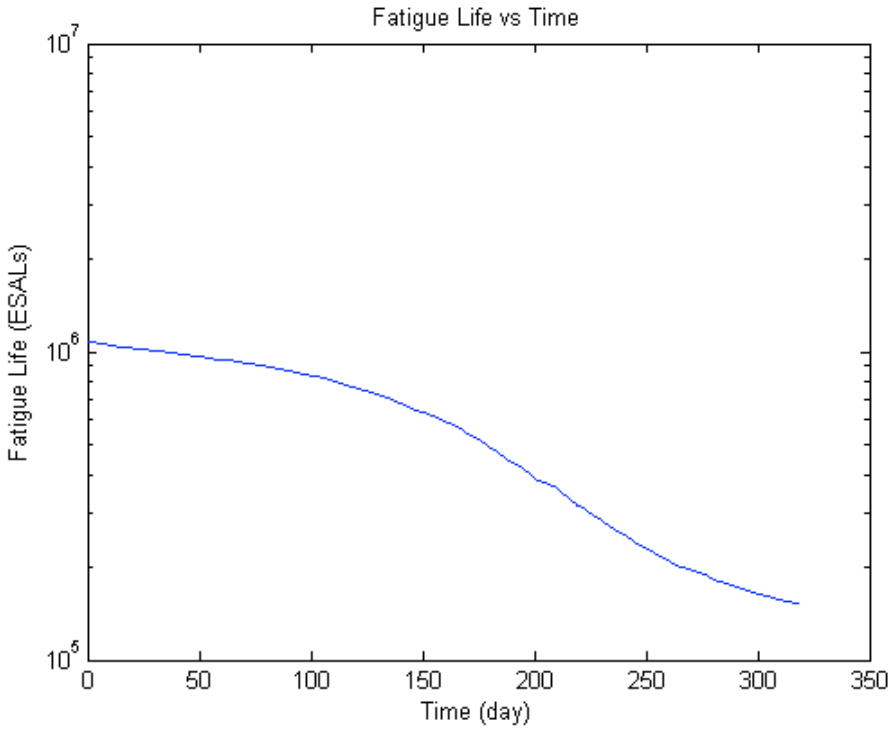

FIGURE 4-5 Fatigue life decline with time for a whole year.

Summary

In this chapter, the software interface of Pavement Aging and Fatigue Analyzer (PAFA) is explained in detail with an illustrative case study. Input for the software requires extensive binder and mixture tests as well as collection of pavement temperature data. Outputs are plots of carbonyl area, DSR function, and fatigue life as a function of time. Numerical results are also saved in a spreadsheet.

The computing engine in the software still needs further improvement. First, fast-rate kinetics of carbonyl formation needs further understanding and implementation. Second, the CMSE approach is being revised in a recent TxDOT project 0-6009 (*27*), which will relate binder aging to more fundamental mixture properties. The results of

that revision will be updated in the software. Last but not least, the effect of moisture damage might be incorporated into the software.

CHAPTER V

SUPPLEMENTAL DATA FOR SOFTWARE

Supplemental data are collected from literature for easy application of the Pavement Aging and Fatigue Analyzer developed in Chapter IV. They also give users a reference for magnitude of different parameters. Presented data include binder kinetics data, mixture tests data and pavement structure information.

Binder Constant-Rate Kinetics Data

Most of constant-rate kinetics data are collected from TxDOT project 1872 (9) and published papers (*3, 14*). Activation energy E_a, pre-exponential factor A, and reaction order with respect to oxygen partial pressure α for constant-rate aging are listed in the Table 5-1.

TABLE 5-1 Constant-rate Kinetics Data at 0.2 atm Oxygen Pressure

Binder Type	**E_a** (KJ/mol)	**Ln(A)** $\mathrm{Ln}(\mathrm{CA/s \cdot atm}^{\alpha})$	**α**
SHRP AAA-1*	108.6	33.28	0.604
SHRP AAB-1*	103.2	31.60	0.426
SHRP AAD-1*	100.2	30.59	0.611
SHRP AAF-1*	75.1	22.06	0.340
SHRP AAG-1*	70.3	20.71	0.279
SHRP AAM-1*	67.5	19.43	0.260
SHRP AAS-1*	105.0	31.98	0.445
Ampet AC-20#	74.8	21.71	0.285
Coastal AC-20#	80.5	23.83	0.266
Cosden AC-20#	68.6	19.86	0.270
Exxon AC-20#	66.7	19.86	0.255
Texaco AC-20#	71.1	20.42	0.250
TX1★	102.1	31.29	0.421
TX2★	101.5	31.06	0.429

* Data from TxDOT project 1872 (9).
# Data from Lunsford (14).
★ Data from Liu (3).

Binder Fast-Rate Kinetics Data

Data for fast-rate kinetics are collected from Herrington's paper (*22*). Herrington aged two types of binder at 60, 70 and 80 °C, at about 2 MPa air pressure. Viscosity data were measured and fit with to Equation 2-1 proposed in chapter II. The following kinetics parameters in Table 5-2 are reported after nonlinear regression analysis of viscosity data.

TABLE 5-2 Viscosity Hardening Kinetics Data*

Binder Type	**Aging Temperature** (°C)	**$K_s \times 10^4$** (hr^{-1})	**K_f** (hr^{-1})	**P_f** (Log Pa•s)	**R^2** (%)
S180	60	5.1	0.019	0.59	98
	70	19.9	0047	0.57	100
	80	59.5	0.109	0.54	99
I180	60	6.4	0.021	0.84	99
	70	18.3	0.046	0.88	100
	80	47.1	0.072	0.85	100

*Because viscosity is measured using glass capillary viscometer, exact shear rate is undetermined. However, it is assumed that shear rate is low enough to treat viscosity measured as low shear rate limiting viscosity.

Other Binder Information

Other binder information includes initial carbonyl area (CA_0), initial viscosity, viscosity hardening susceptibility (HS), initial DSR function, DSR function HS, and oxygen diffusivity. Experimental data are listed in Table 5-3 through Table 5-7.

TABLE 5-3 Initial Carbonyl Area Data

Binder Type	CA_0	Comment
SHRP AAG-1*	1.275	Constant-rate intercept
PG 64-22 (Bryan)#	0.807	Binder of Bryan mixture, after PP2
PG 76-22 +SBS (B1)#	0.720	Binder of B1 mixture, after PP2
PG 76-22 +TR (C1)#	0.7175	Binder of C1 mixture, after PP2

* Data from TxDOT project 1872 (9).
# Data from TxDOT project 0-4468 (17, 18).

TABLE 5-4 Initial Viscosity (@60 C and 0.1 rad/s)

Asphalt Binder	Viscosity (poise)[1]
SHRP AAA-1*	1081
SHRP AAD-1*	1366
SHRP AAF-1*	2261
SHRP AAS-1*	3162
SHRP ABM-1*	3313
Conoco AC-20*	3870
Exxon AC-10*	1203
Exxon AC-20*	2267
GSAC AC-15P Base*	858
Shell AC-20*	2232
PG 64-22 (Bryan)#	37550

* Data from TxDOT project 1872 (9).
# Data from TxDOT project 0-4468 (17).

TABLE 5-5 Viscosity Hardening Susceptibility of Asphalt Binder*

Binder Type	Hardening Susceptibility (Ln(poise)/CA)
Fina AC-5	4.61
Fina AC-5 2% SBR	3.77
Fina AC-10	3.96
Fina AC-10 2% SBR	3.71
Fina AC-20	4.32
Fina AC-20 1% SBR	3.66

* Data from TxDOT project 1872 (9).

[1] NOTE: 1 poise = 0.1 Pa•s

TABLE 5-5 Continued

Binder Type	**Hardening Susceptibility** (Ln(poise)/CA)
Wright AC-10*	5.38
Wright AC-10 2% SBR*	4.94
Wright AC-10 3% SBR*	4.01
Wright AC-10 3% SBS*	5.02
Wright AC-20*	6.09
Wright AC-20 3% SBR*	4.20
Wright AC-20 3% SBS*	4.84
Wright AC-20 2~5% SBS 5% Tire Rubber*	2.53
TFA AC-20*	7.90
TFA AC-20 3% SBR*	4.52
Exxon AC-30*	5.71
Exxon Base 1% SBR*	4.98
UR AC-10*	3.89
UR AC-10 3% SBR*	2.85
GSAC AC-10*	2.94
GSAC AC-10 3% SBS*	2.21
PG 64-22 (Bryan)#	6.93

* Data from TxDOT project 1872 (9).
# Data from TxDOT project 0-4468 (17).

TABLE 5-6 Initial DSR Function and Hardening Susceptibility

Asphalt Binder	**DSR Function × 10^9** (MPa/s)	**DSR Function HS** (Ln(MPa/s)/CA)
AAA-1*	88.35	8.61
AAB-1*	1103	6.26
AAD-1*	7.60	9.49
AAF-1*	3874	6.08
ABM-1*	356.9	4.35
AAM-1*	9602	4.39
AAS-1*	6375	4.70
Lau4*	862.4	6.68
TS2K*	394.5	5.83
PG 64-22 (Bryan)#	211000	8.95
PG 76-22SBS(B1)#	278000	6.34
PG 76-22TR(C1)#	163000	7.28

* Data from TxDOT project 1872 (9).
# Data from TxDOT project 0-4468 (17, 18).

TABLE 5-7 Oxygen Diffusivity in Asphalt Binder*

Asphalt Binder	**Oxygen Diffusivity × 10^{13}** (m^2/s)
Ampet AC-20	20.0
Coastal AC-20	64.9
Cosden AC-20	20.0
Exxon AC-20	150.0
Texaco AC-20	38.9

*Assume oxygen pressure as 0.27 atm. Data from Lunsford (14).

Mixture Information

Mixture data include mixture design, mixture test results and shift factors of unaged mixture. This data are listed in Tables 5-8 through 5-13.

TABLE 5-8 Mixture Design and Notation*

Mixture Notation	**Binder Type + Modifier**	**Binder Content (by weight of mix)**	**Aggregate Type**
Bryan	PG 64-22	4.4%	Limestone
A1	PG 64-22	5.0%	Gravel
A2	PG 64-22	5.5%	Gravel
B1	PG 76-22 + SBS	5.3%	Gravel
B2	PG 76-22 + SBS	5.8%	Gravel
C1	PG 76-22 + TR	5.2%	Gravel
C2	PG 76-22 + TR	5.7%	Gravel

* Data from TxDOT project 0-4468 (17, 18).

TABLE 5-9 Mixture Tensile Strength Test Results*

Mixture Notation	**Tensile Strength** (psi)[2]
Bryan	105
A1	76
A2	68
B1	123
B2	115
C1	125
C2	112

* Data from TxDOT project 0-4468 (17, 18).

[2] NOTE: 1 psi = 6.89 kPa

TABLE 5-10 Mixture Relaxation Modulus Test Results*

Mixture Notation	**Relaxation Modulus** (psi)	**Rate of Stress Relaxation**
Bryan	208,100	0.4
A1	185,000	0.55
A2	143,000	0.72
B1	178,785	0.51
B2	185,000	0.59
C1	210,000	0.4
C2	205,000	0.48

* Data from TxDOT project 0-4468 (17, 18).

TABLE 5-11 Mixture Repeated Direct Tension Test Results*

Mixture Notation	**Rate of Damage Accumulation**
Bryan	0.8
A1	0.5
A2	0.47
B1	0.68
B2	0.45
C1	0.87
C2	0.85

* Data from TxDOT project 0-4468 (17, 18).

TABLE 5-12 Mixture Fracture Surface Energy Test Results*

Mixture Notation	**Fracture Surface Energy** (ergs/cm^2)[3]
Bryan	166
A1	181
A2	181
B1	253
B2	253
C1	248
C2	248

* Data from TxDOT project 0-4468 (17, 18).

[3] NOTE: 1 ergs/cm^2 = 0.001 J/m^3

TABLE 5-13 Shift Factors of Unaged Mixture*

Mixture Notation	Healing Shift Factor	Anisotropy Shift Factor
Bryan	6.73	2.0
A1	7.18	2.0
A2	7.28	2.0
B1	7.26	2.0
B2	7.32	2.0
C1	5.91	2.0
C2	6.53	2.0

* Data from TxDOT project 4468 (17, 18).

CHAPTER VI

SUMMARY AND RECOMMENDATIONS

Summary

In Chapter I, recent research findings on binder oxidation and mixture fatigue characterization are reviewed. Binder kinetics and oxygen transport model with pavement temperature input provide the bases for prediction of binder aging in pavement. By assuming an empirical relationship between fatigue life decline and binder aging, specifically DSR function, fatigue life can be predicted using the CMSE approach for fatigue analysis.

Fast-rate binder oxidation kinetics was investigated in Chapter II. One unmodified binder SEM 64-22 and one SBS-modified binder SEM 70-22 were aged at five elevated temperatures and air pressure. Carbonyl area data were measured and analyzed. While the proposed parallel reaction model fits data of SEM 64-22, especially for low-temperature data, it does not fit data of SEM 70-22. Polymer modification might be responsible for this discrepancy. Nonetheless, more data are required to draw any conclusions.

In Chapter III, a new pattern-based model was developed for hourly air temperature using time series analysis. The new method consistently yields better results than the conventional sinusoidal model. Accurate hourly air temperature is needed as an input for model prediction of hourly pavement temperature.

In Chapter IV, pavement aging and fatigue analysis (PAFA) software was developed, which utilizes research findings discussed in the previous two chapters. The

software offers a graphic interface for various inputs. Inputs are organized into three categories: 1) binder information, 2) mixture information, and 3) field information. After running the program, carbonyl area and DSR function of binder and fatigue life of mixture are plotted as a function of time. Output data are saved in spreadsheet.

Experimental data from literature are tabulated in Chapter V as supplement for PAFA developed in Chapter IV.

Recommended Further Research

The oxidation kinetics of binders during the early fast-rate period requires further research. Also, fundamental understanding of binder aging effect on mixture fatigue performance, instead of an empirical relationship, is desirable. Research on these two subjects is underway in TxDOT project 0-6009 (*27*). Findings of this project will be followed closely and implemented in a newer version of PAFA software. Furthermore, a sensitivity analysis of various inputs with respect to PAFA software output is also an interesting subject for identification of the importance of these inputs.

REFERENCES

1. U.S. Department of Transportation, Federal Highway Administration. *Highway Statistics 2007.* www.fhwa.dot.gov/policyinformation/statistics/2007/index.cfm. Accessed Mar. 16, 2009.

2. Mirza, M.W. and M.W. Witczak. Development of a Global Aging System Short and Long Term Aging of Asphalt Cements. *Journal of the Association of Asphalt Paving Technologists*, Vol. 64, 1995, pp. 393-430.

3. Liu, M., K. M. Lunsford, R. R. Davison, C. J. Glover, and J. A. Bullin. The Kinetics of Carbonyl Formation in Asphalt. *AIChE J.*, Vol. 42, No. 4, 1996.

4. Al-Azri, Nasser A., Sung Hoon Jung, Kevin M. Lunsford, Ann Ferry, Jerry A. Bullin, Richard R. Davison, and Charles J. Glover. Binder Oxidative Aging in Texas Pavements − Hardening Rates, Hardening Susceptibilities, and Impact of Pavement Depth. In *Transportation Research Record: Journal of the Transportation Research Board, No. 1962*, Transportation Research Board of the National Academies, Washington, DC, 2006, pp. 12–20.

5. Lytton, R. L., J. Uzan, E. G. Fernando, R. Roque, D. Hiltunen, and S. Stoffels. *Development and Validation of Performance Prediction Models and Specifications for Asphalt Binders and Paving Mixes*. Publication SHRP-A-357. Strategic Highway Research Program, National Research Council Washington, DC, 1993.

6. Wiehe, I. A. and K. S. Liang. Asphaltene, Resin, and Other Petroleum Macromolecules, *Fluid Phase Equil.*, Vol.117, 1996, pp. 201-210.

7. Petersen J. C. and P. M. Harnsberger. Asphalt Aging − Dual Oxidation Mechanism and Its Interrelationships with Asphalt Composition and Oxidative Age Hardening. In *Transportation Research Record: Journal of the Transportation Research Board, No. 1638*, Transportation Research Board of the National Academies, Washington, DC, 1998, pp. 47–55.

8. Domke, C. H., R. R. Davison, and C. J. Glover. Effect of Oxidation Pressure on Asphalt Hardening Susceptibility. In *Transportation Research Record: Journal of the Transportation Research Board, No. 1661*, Transportation Research Board of the National Academies, Washington, DC, 1999, pp. 114-121.

9. Glover, C. J., R. R. Davison, C. H. Domke, Y. Ruan, P. Juristyarini, D. B. Knorr, and S. H. Jung. *Development of a New Method for Assessing Asphalt Binder Durability with Field Validation*. Publication FHWA/TX-05/1872-2. Texas Transportation Institute, College Station, TX, 2005.

10. Carslaw, H. S., and J. C. Jaeger. *Conduction of Heat in Solids, 2nd edition.* Oxford Science Publications, New York, 1959.

11. Diefenderfer, B. K., A. M. Asce, I. L. AL-Qadi, and S. D. Diefenderfer. Model to Predict Pavement Temperature Profile: Development and Validation. *J. Transp. Eng.*, Vol. 132, 2006, pp.162-167.

12. Hermansson, A. Simulation model for calculating pavement temperatures, including maximum temperature. In *Transportation Research Record: Journal of the Transportation Research Board, No. 1699*, Transportation Research Board of the National Academies, Washington, DC, 2000, pp. 134–141.

13. Hermansson, A. Mathematical Model for Paved Surface Summer and Winter Temperature: Comparison of Calculated and Measured Temperatures. *Cold Reg. Sci. Technol.*, Vol. 40, 2004, pp. 1-17.

14. Lunsford, K. M. *The Effect of Temperature and Pressure on Laboratory Oxidized Asphalt Films with Comparison to Field Aging*. Ph.D. Dissertation. Texas A&M University, College Station, TX, 1994.

15. Al-Omari, A., L. Tashman, E. Masad, L. A. Cooley, Jr. and T. Harman. Proposed Methodology for Predicting HMA Permeability. *Journal of the Association of Asphalt Paving Technologists*, Vol. 71, 2002, pp. 30-58.

16. Prapaitrakul, N., R. Han, X. Jin and C. J. Glover. A Transport Model of Asphalt Binder Oxidation in Pavements. *Road Materials and Pavement Design*, 2009. Submitted.

17. Walubita, L. F., A. Epps Martin, S. H. Jung, C. J. Glover, E. S. Park, A. Chowdhury, and R. L. Lytton. *Comparison of Fatigue Analysis Approaches for Two Hot Mix Asphalt Concrete (HMA) Mixtures*. Publication FHWA/TX-05/0-4468-2. Texas Transportation Institute, College Station, TX, 2005.

18. Walubita, L. F., A. Epps Martin, S. H. Jung, C. J. Glover and E. S. Park. *Application of Calibrated Mechanistic Fatigue Analysis with Aging Effects.* Publication FHWA/TX-06/0-4468-3. Texas Transportation Institute, College Station, TX, 2006.

19. Woo, W. J., E. Ofori-Abebresse, A. Chowdhury, J. Hilbrich, Z. Kraus, A. Epps Martin, and C. J. Glover. *Polymer Modified Asphalt Durability in Pavements*. Report FHWA/TX-07/0-4688-1. Texas Transportation Institute, College Station, TX, 2007.

20. Van Oort, W.P. Durability of Asphalt. *Industrial and Engineering Chemistry*, 1956, pp. 1196-1201.

21. Dickinson, E. J. and J. H. Nicholas. The Reaction of Oxygen with Tar Oils. *Road Research, Technical Paper*, No. 16, 1949.

22. Herrington, P. R. Oxidation of Bitumen in the Presence of a Constant Concentration of Oxygen. *Petroleum Science and Technology*, Vol. 16, No. 9-10, 1998, pp. 1061-1084.

23. Lau, C. K., K. M. Lunsford, C. J. Glover, R. R. Davison, and J. A. Bullin. Reaction Rates and Hardening Susceptibilities as Determined from POV Aging of Asphalts. In *Transportation Research Record: Journal of the Transportation Research Board, No. 1342*, Transportation Research Board of the National Academies, Washington, DC, 1992, pp. 50-57.

24. Debele, B., R. Srinivasan and J. Y. Parlange. Accuracy Evaluation of Weather Data Generation and Disaggregation Methods at Finder Timescales. *Advances in Water Resources*, Vol. 30, 2007, pp. 1286-1300.

25. Brockwell, P. J. and R. A. Davis. *Introduction to Time Series and Forecasting,* Second Edition. Springer-Verlag, New York, 2002.

26. AASHTO Designation: PP2. Standard Practice for Short and Long Term Aging of Hot Mix Asphalt. *AASHTO Provisional Standards*. Washington, D.C June Edition. 1994.

27. Glover, C. J., A. Epps Martin, A. Chowdhury, R. Han, N. Prapaitrakul, X. Jin, and J. Lawrence. *Evaluation of Binder Aging and Its Influence in Aging of Hot Mix Asphalt Concrete: Literature Review and Experimental Design*. Publication FHWA/TX-08/0-6009-1. Texas Transportation Institute, College Station, TX, 2009.

VITA

Name: Xin Jin

Address: Department of Chemical Engineering
c/o Dr. Charles Glover
Texas A&M University
College Station, TX 77843-3122

Email Address: xin.jin@tamu.edu

Education: B. E., Automation, Zhejiang University, China, 2005